Form Approved
OBM No. 0704-0188

1. Agency	1992	3. Report Type and Dates Covered. Final - Book Contribution

(2)

4. Title and Subtitle.
Chapter 22. The Use of Satellite Observations in Ice Cover Simulations

5. Funding Numbers.
Program Element No. 0602435N
Project No. RM35G94
Task No. 801
Accession No. DN251065
Work Unit No. 13222A

6. Author(s).
Ruth H. Preller, John E. Walsh*, and James A. Maslanik**

7. Performing Organization Name(s) and Address(es).
Naval Research Laboratory
Oceanography Division
Stennis Space Center, MS 39529-5004

8. Performing Organization Report Number.
BC 001-92-322

9. Sponsoring/Monitoring Agency Name(s) and Address(es).
Office of Naval Research
800 N. Quincy St.
Arlington, VA 22217

10. Sponsoring/Monitoring Agency Report Number.
BC 001-92-322

11. Supplementary Notes.
Published in Microwave Remote Sensing of Sea Ice.
*University of Illinois, Urbana, IL 61801, **University of Colorado, Boulder, CO.

12a. Distribution/Availability Statement.
Approved for public release; distribution is unlimited.

12b. Distribution Code.

13. Abstract *(Maximum 200 words).*

The combination of numerical models and observational data can provide a unique tool for studying the complex interactions of the atmosphere, the ice, and the ocean. The formulation of numerical ice and coupled ice-ocean-atmosphere models is based on our knowledge of dynamic and thermodynamic principles and how they relate to observed ice conditions. Field experiments such as the Arctic Ice Dynamics Experiment (AIDJEX) [Pritchard, 1980] and the Marginal Ice Zone Experiment (MIZEX) [*Journal of Geophysical Research Oceans, 88(C5), 92(C7), 96(C3)*] have provided observational data from which the basis of many of the formulations for ice drift, internal ice stresses, heat exchange, etc., have come. Numerical models, on the other hand, may be used to provide information on ice drift, ice thickness, and ice concentration in regions where observations are scarce or missing. In addition, numerical models may be used to forecast ice conditions.

14. Subject Terms.
Ice model development, data analysis and assimilation, model evaluation

15. Number of Pages.
20

16. Price Code.

17. Security Classification of Report.	18. Security Classification of This Page.	19. Security Classification of Abstract.	20. Limitation of Abstract.
Unclassified	Unclassified	Unclassified	SAR

Chapter 22. The Use of Satellite Observations in Ice Cover Simulations

RUTH H. PRELLER
Naval Research Laboratories, Stennis Space Center, Mississippi 39529-5004

JOHN E. WALSH
Department of Atmospheric Sciences, University of Illinois, 105 South Gregory Avenue, Urbana, Illinois 61801

JAMES A. MASLANIK
Cooperative Institute for Research in Environmental Sciences, University of Colorado, Boulder, Colorado 80309

22.1 INTRODUCTION

The combination of numerical models and observational data can provide a unique tool for studying the complex interactions of the atmosphere, the ice, and the ocean. The formulation of numerical ice and coupled ice–ocean–atmosphere models is based on our knowledge of dynamic and thermodynamic principles and how they relate to observed ice conditions. Field experiments such as the Arctic Ice Dynamics Experiment (AIDJEX) [Pritchard, 1980] and the Marginal Ice Zone Experiment (MIZEX) [*Journal of Geophysical Research Oceans, 88(C5), 92(C7), 96(C3)*] have provided observational data from which the basis of many of the formulations for ice drift, internal ice stresses, heat exchange, etc., have come. Numerical models, on the other hand, may be used to provide information on ice drift, ice thickness, and ice concentration in regions where observations are scarce or missing. In addition, numerical models may be used to forecast ice conditions.

Satellites have been able to provide observational data over larger areas and for longer periods of time than from conventional observations. Since 1972, passive microwave data from polar orbiting satellites have provided large-scale coverage of Arctic and Antarctic sea ice on a nearly continuous basis at resolutions as fine as 25 km. Visible and infrared imagery provide higher resolution data than the passive microwave, but do not have the all-weather capability that the passive microwave data have. A very promising source of high-resolution, all-weather data is the satellite-borne Synthetic Aperture Radar (SAR). Data from this instrument have recently become available via the launch of the ERS-1 satellite on July 17, 1991.

With the recent availability of larger amounts of satellite data in ice covered regions and the continuous development of more advanced numerical models for these regions, the logical next step is merging the data with the models. This merger will most likely occur through expanded use of data assimilation into the models. This combination should provide the best available analysis and forecast of ice conditions, as well as improve our understanding of dynamic and thermodynamic interactions in the ice. In addition, models are likely to be used more extensively to improve data processing algorithms and to help interpret complex responses recorded in the data.

Microwave Remote Sensing of Sea Ice
Geophysical Monograph 68

22.2 NUMERICAL MODELS

22.2.1 *Ice Models—Dynamic, Thermodynamic, and Dynamic-Thermodynamic*

Numerical models of sea ice, developed over approximately the last twenty years, may be broken down into three categories: dynamic, thermodynamic, and dynamic-thermodynamic ice models.

Dynamic ice models use the various stresses on the ice to define the motion of the ice. The momentum balance used in dynamic ice models is

$$m\frac{\delta}{\delta t}\vec{u} = -mf\hat{k}\times\vec{u} + \vec{\tau}_a + \vec{\tau}_w - mg\,\mathrm{grad}H + \vec{F} \qquad (1)$$

where m is the ice mass per unit area and $\vec{u}$ is the ice drift velocity. The terms on the right side of the equation are the Coriolis term (where f is the Coriolis parameter), the wind stress on ice $\vec{\tau}_a$, the ocean stress on ice $\vec{\tau}_w$, the acceleration due to sea surface tilt $mg\,\mathrm{grad}H$ (where H is the sea surface dynamic height), and the internal ice stress term $\vec{F}$.

The simplest of the dynamic models, the free drift model, uses a balance between top and bottom surface stresses and the Coriolis force to determine ice motion. Free drift is often a good approximation away from boundaries and under divergent conditions. Removal of the last term in Equation (1), the effect of internal ice stress, results in the free drift balance. Ice drift may be significantly adjusted in both magnitude and direction by the internal ice stress that generally acts in a direction opposite to the resultant of the wind stress and Coriolis force. Models that include internal ice stress contain a constitutive law that treats ice as a viscous, elastic, viscous-plastic, or elastic-plastic medium.

In a viscous rheology, stress can only be sustained through a nonrecoverable dissipation of energy by deformation. A plastic rheology allows stress to be sustained through a lack of deformation or elastic deformation in which the energy is recoverable. A linear viscous rheology in which stress depends on linear strain rates and a rigid plastic rheology in which the stress state is either dependent on the magnitude of the strain rates or indeterminate are two special case rheologies often used to describe sea ice. For a more detailed review of these constitutive laws, see Hibler [1980b, 1986].

An intermediate approach with considerable promise for climate simulations is the cavitating fluid approximation, which differs from free drift by allowing nonzero ice pressure under converging conditions, but, like free drift, offers no resistance to divergence or shear [Flato and Hibler, 1989]. In the corresponding numerical procedure, free-drift velocities are corrected iteratively in a momentum-conserving way.

Thermodynamic ice models take into account the interactions of both the atmospheric and oceanic heat fluxes with the ice to determine ice growth and decay. Many of the formulations of sea ice thermodynamics used in numerical ice models are based on the work of Maykut and Untersteiner [1971]. Figure 22-1 depicts the one-dimensional snow–ice–water system they use. The heat fluxes from the atmosphere and ocean are passed into the snow and ice by conduction.

At the snow–air surface, the balance of heat fluxes is given by

$$(1-\alpha)F_r - I_0 + F_L - \varepsilon\sigma T^4 + F_s + F_e + K_0\left(\frac{\partial T}{\partial z}\right)_0 = \begin{cases} 0 \text{ if } T \le 273 \text{ K} \\ -q\left(\frac{\partial}{\partial t}\right)(S+h) \text{ if } T \ge 273 \text{ K} \end{cases} \quad (2)$$

where α is the albedo, F_r is the solar (shortwave) radiation, and I_0 is the flux of shortwave radiation through the surface into the ice, assumed by Maykut and Untersteiner to be 17% of the net shortwave radiation at the surface. The term F_L is the incoming longwave radiation from the atmosphere (clouds) and $\varepsilon\sigma T^4$ is the outgoing longwave radiation based on the surface temperature, where ε is the longwave emissivity, σ is the Stefan–Boltzmann constant, and T is the surface temperature. Then, F_s is the sensible heat flux, F_e is the latent heat flux, K is the thermal conductivity, q is the latent heat of fusion, z is the depth within the ice–snow column, and $\partial(S+h)/\partial t$ is the ablation rate of snow and ice where S is the thickness of the snow and h is the thickness of the ice. The subscript 0 generically refers to the upper surface. At the snow–ice interface, the balance of fluxes is

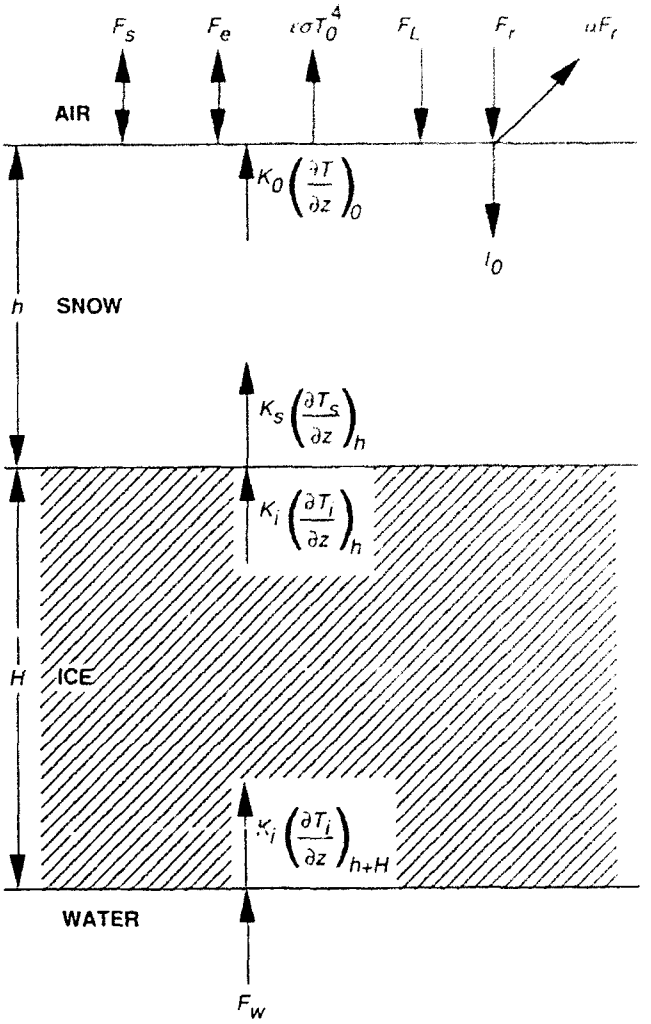

Fig. 22-1. The one-dimensional snow–ice–water system used by Maykut and Untersteiner [1971].

$$K_s\frac{\partial T_s}{\partial z} = K_i\frac{\partial T_i}{\partial z} \quad (3)$$

The subscripts s and i stand for snow and ice, respectively. At the ice–ocean interface the balance is

$$K_i\frac{\partial T_i}{\partial z} = F_w - q\frac{\partial}{\partial t}(S+h) \quad (4)$$

where F_w is the oceanic heat flux.

Thermal conductivity, specific heat, and ice density are all functions of salinity and temperature. This dependency is due in large part to brine pockets in the ice. Brine pockets can act as thermal reservoirs and slow down the heating or cooling of ice. Since brine has a small conductivity and greater specific heat than ice, the parameters also vary with temperature.

To calculate heat conduction, the diffusion equation for temperature is given by

$$(\rho c)_i \frac{\partial T_i}{\partial t} = K_i \frac{\partial^2 T_i}{\partial z^2} + k_i I_0 \exp(-k_i z) \quad (5)$$

where k is the bulk extinction coefficient and c is the heat capacity. In snow, K and k are constant and I_0 is set equal to zero. In ice, K and k can vary due to the effects of brine pockets as noted above [Untersteiner, 1961].

Although the Maykut and Untersteiner model provides a thorough treatment of the snow–ice thermodynamic system, the complexity of the model can make it impractical for modeling large areas. Semtner [1976] simplified the Maykut and Untersteiner model by fixing the snow and ice conductivities. The salinity profile, required by the Maykut and Untersteiner model, does not have to be specified in Semtner's version. Internal melting is attributed to an amount of penetrating radiation stored in a heat reservoir without causing ablation. Energy from this reservoir keeps the temperature near the ice surface from dropping below freezing in the fall. Semtner's model was further simplified by assuming linear equilibrium temperature gradients in the snow and ice. The heat flux is uniform in both the ice and snow. No temperature flux exists at the snow–ice surface. The surface heat balance is set equal to zero and is used to solve for the surface temperature.

The third category, the dynamic-thermodynamic model, integrates ice motion and ice growth and decay effects into one model. Parkinson and Washington [1979] designed one of the first three-dimensional dynamic-thermodynamic models. Within each grid cell, the model was broken down vertically into four layers: a mixed layer ocean, an ice layer, a snow layer, and an atmospheric boundary layer. At the ice–ocean interface, geostrophic ocean currents were used to supply ocean stress to the ice. A temporarily invariant dynamic topography and a constant oceanic heat flux were prescribed. Atmospheric heat fluxes and wind stress were applied at the air–ice interface. The ice drift, derived from a free-drift formulation, was iteratively corrected to insure the existence of a minimum fraction of leads. This iteration does not conserve momentum and can damp the ice drift.

A more realistic treatment of ice dynamics was used by Hibler [1979]. This model uses a viscous-plastic constitutive law. A plastic rheology is used to relate the strength of ice interaction to a two-level ice thickness distribution. The ice strength P is defined by

$$P = P^* h \, e^{-C(1-A)} \quad (6)$$

where A is the ice compactness or concentration and P^* and C are constants. Ice concentration is defined in these models as the fraction of a grid cell that is covered by thick ice. The area covered by thin ice or open water is $1 - A$. Equation (6) allows the ice strength to be greater in regions of ice inflow and weaker in regions of ice outflow.

The model also incorporates the equations of continuity for ice concentration and thickness defined as

$$\frac{\partial h}{\partial t} = -\frac{\partial (uh)}{\partial x} - \frac{\partial (vh)}{\partial y} + S_h + (\text{Diffusion}) \quad (7)$$

$$\frac{\partial A}{\partial t} = -\frac{\partial (uA)}{\partial x} - \frac{\partial (vA)}{\partial y} + S_A + (\text{Diffusion}) \quad (8)$$

where S_h and S_A are source and sink terms accounting for the growth and melt of ice. In later papers [e.g., Hibler, 1980a], these growth rates were calculated, as opposed to prescribed, from the heat budget balance similar to that used by Parkinson and Washington [1979].

Snow cover was not included explicitly in the Hibler ice model. Instead, based on the work of Bryan et al. [1975] and Manabe et al. [1979], the effects of snow cover were approximated by setting the ice surface albedo to that of snow when the surface temperature was below freezing and to that of snow-free ice when the surface was at the melting point. Walsh et al. [1985] were the first to include snow explicitly in a long-term simulation using daily winds and air temperature data from the National Center for Atmospheric Research (NCAR) for the years 1951 through 1980. In this model, both snow and ice were composed of seven thickness levels. The seven levels were defined by taking twice the average ice or snow thickness within a grid cell and dividing it into seven equal levels. The growth and melt of the ice and snow, based on the heat budget balance, was calculated at each level and then averaged back into one thick ice growth rate. Snowfall rates consisted of monthly varying climatological rates from Maykut and Untersteiner [1971]. In this system, heat from the heat budget balance is used to melt all the snow before it is used to melt ice. If a snow cover exists, the albedo is set to 0.80. When there is no snow, the albedo is 0.65. A version of the Hibler ice model, similar to that used by Walsh et al. [1985], is presently used as the basis for the Polar Ice Prediction System (PIPS), the U.S. Navy's numerical sea-ice forecast model.

22.2.2 Ice–Ocean Models

The development of models for ice covered regions was further expanded by including the temporal and spatial variability of the ocean. This was accomplished by fully coupling ice to ocean models. The first fully coupled, three-dimensional model was designed by Hibler and Bryan [1984, 1987]. The model coupled the Hibler ice model to the Bryan–Cox multilevel ocean model [Bryan, 1969] both dynamically and thermodynamically. The ocean model was initialized from climatological temperatures and salinities and weakly constrained to those values with a three-year relaxation period. Tests performed using this model highlighted the importance of the deep-ocean heat flux into the mixed layer. This heat is great enough to keep parts of the

Barents and Greenland Seas ice-free all winter. Semtner [1987] used a similar coupled ice–ocean model, but removed the constraint on the ocean temperature and salinity. He also used simplified ice dynamics that contained only bulk viscosity (no shear). Semtner's results verified the importance of the oceanic heat flux on keeping the marginal ice zone ice-free in winter. However, his ice thickness distribution contained thinner ice than found by Hibler and Bryan. Fleming and Semtner [1991] reduced the ice strength used by Semtner [1987] and obtained a much more realistic ice thickness distribution. Riedlinger and Preller [1991] used a model similar to the Hibler and Bryan model, but used daily varying forcing from the Navy's operational global atmospheric model. This study showed that the diagnostic ocean model could provide a useful tool for forecasting.

Additional ice–ocean models have been developed that show the importance of including a mixed layer in the ocean. One-dimensional models [Pollard et al., 1983; Lemke and Manley, 1984; Ikeda, 1985; Lemke, 1987; Bjork, 1989; Mellor and Kantha, 1989; Riedlinger and Warn–Varnas, 1990], two-dimensional models [Kantha and Mellor, 1989], and three-dimensional models [Piacsek et al., 1991] have all shown distinct changes to the heat and salt exchange (and therefore the ice growth and decay rates) when a mixed layer is included.

These dynamic-thermodynamic ice and ice–ocean models have mainly been applied to large-scale simulations using grid resolutions on the order of 100 km. The Hibler ice model has been applied, however, on regional scales to the Greenland Sea [Tucker, 1982; Preller et al., 1990] and to the Barents Sea [Preller et al., 1989] at grid resolutions of approximately 20 km.

Higher resolution models (of a few kilometers) have often been used to look at processes normally associated with the region near the ice edge. Roed and O'Brien [1983] and Hakkinen [1986] used one- and two-dimensional ice–ocean models, respectively, to study upwelling at the ice edge. Ikeda [1988] used a three-dimensional ice–ocean model that included thermodynamics to investigate upwelling at the ice edge. Tang [1991] used a two-dimensional thermodynamic ice–ocean model to study the advance and retreat of the ice edge near Newfoundland. Smith et al. [1988] used a three-dimensional, two-layer ocean model coupled to a Hibler-type ice model to investigate the behavior of an isolated ocean eddy within the marginal ice zone. Smith and Bird [1991] used the same model to study the interaction of an ocean eddy with a jet at the ice edge.

22.2.3 *Ice–Atmosphere Models*

Because ice–atmosphere interaction cannot be divorced from the ocean's influence, there have been relatively few studies utilizing interactive models of only the atmosphere and sea ice. The studies that fall into this category have generally been one- or two-dimensional experiments with energy balance models. Such studies have tended to focus on the effects of specific processes. For example, Ledley [1988, 1991] has used a coupled energy-balance sea-ice model to examine the effects of prescribed lead fractions, snowfall, and a highly parameterized transport of sea ice. Ledley's model is one-dimensional (latitudinal), but it does include a partitioning of each latitudinal zone into land and ocean. Harvey [1988] developed a more comprehensive sea ice model for use in zonally averaged energy-balance climate simulations. Harvey's model, which includes parameterizations of processes such as surface and lateral melting, leads, advection, and snow and ice thickness distributions, has been used to study various sea ice feedbacks (albedo, leads, etc.). Although models such as these are so highly idealized that their relevance to the actual climate system is unclear, they do identify high-leverage parameters and processes that merit further study with more sophisticated models.

Ice–atmosphere models have also been used to study atmospheric boundary layer processes and interactions at the air–ice interface. Overland [1985], for example, used an atmospheric boundary layer model to address momentum exchange and surface drag parameterizations at the air–ice interface. Bennett and Hunkins [1986] used a two-dimensional model to examine atmospheric boundary-layer modifications during advection over an inhomogeneous sea ice cover. Pease and Overland [1984] studied the drift and mass balance of sea ice in the Bering Sea by using an atmospherically driven sea ice model.

22.2.4 *Linkage to General Circulation Models*

A survey of current versions of the general circulation models (GCM's) used to simulate the global climate reveals a substantial gap between state-of-the-art sea ice models and the treatment of sea ice in GCM's. Most climate models treat sea ice as a motionless slab characterized by a single thickness in each cell. The simulated sea ice simply accretes or melts in response to a deficit or surplus in the surface energy budget. The treatments that permit sea ice motion do so with relatively crude parameterizations. For example, the model of Manabe and Stouffer [1988] retains the formulation of Bryan [1969], whereby ice moves in the direction of the surface ocean currents until the ice reaches a threshold thickness (4 m), after which ice motion ceases. Few models include leads and open water areas within the pack in spite of the importance of these elements to the atmospheric simulation, as shown in various sensitivity studies (e.g., [Simmonds and Budd, 1990]). The models that do include leads generally prescribe the lead fractions, as discussed below.

The inclusion of ice transport, leads, and open water in interactive models is essential to the realistic simulation of sea ice and climate for several reasons. Areas of thin ice and open water, continually created by deformation, are the sources of nearly all the new ice growth, salt rejection, and heat exchange with the atmosphere. The flux of sensible heat from the ocean to the atmosphere during winter is one to two orders of magnitude greater over thin ice and open

water than over perennial ice. Maykut [1978] has shown that, in an areally averaged sense, a large fraction of the heat transfer from the polar oceans to the atmospheric boundary layer during winter takes place over young ice (thickness ≤0.5 m). The summer melt of ice and the heat storage in the ocean are accelerated dramatically by the absorption of solar radiation in leads and other low-albedo areas such as new ice.

With regard to ice transport, the climatological mean pattern of ice motion across the Arctic Basin and through the Fram Strait results in a net salinity flux to the continental shelves off Siberia. These shelves are regions of net ice growth. The Greenland, Iceland, and Norwegian Seas are regions of net ice melt. The net gain of salt by brine rejection in the shelf waters of the Arctic Ocean is thought to drive the thermohaline circulation of the Arctic Ocean [Aagaard et al., 1985]. The export of sea ice into the North Atlantic subpolar seas is a major source of fresh water for this region, in which deep water formation occurs intermittently and is highly sensitive to the salinity-determined stratification of the ocean surface layers [Aagaard and Carmack, 1989].

Although leads are not determined by ice dynamics in current versions of major GCM's, prescribed or simply parameterized leads have recently been included in several climate simulations. The United Kingdom Meteorological Office (UKMO) and Australian model, for example, have been run with seasonally varying prescribed lead fractions. Sensitivity experiments performed with the Australian model indicate that prescribed lead fractions of 50% in the Antarctic during winter cause the simulated circulation to resemble more closely the case of an ice-free southern ocean than the case of an ice-covered southern ocean [Simmonds and Budd, 1990]. Even when relatively modest lead fractions (several percent) are prescribed in accordance with observations, the atmospheric sea level pressure changes by 5 mb in some high-latitude regions. An alternative strategy has been followed in the Goddard Institute for Space Sciences (GISS) II model [Raymo et al., 1990], which computes a fraction of open water (leads) as $fr = 0.1/Z_{ice}$, where Z_{ice} is the ice thickness in meters. The latter is currently prescribed as 1 m at all times, resulting in a lead fraction of 10%; the use of computed values of Z_{ice} will permit more thorough tests of this parameterization. This parameterization of leads is mentioned here merely to indicate the relatively simplistic nature of such parameterizations in state-of-the-art global climate models.

It should be noted that the ice–ocean interactions involving salinity (freshwater) fluxes will not be reproduced correctly by coupled models until the models include ice transport. While ice transport is simulated well by atmospherically forced ice models (e.g., PIPS), a successful simulation of ice transport in coupled GCM's will require an adequate simulation of the surface wind field and, hence, of the sea level pressure field. There is no evidence yet that atmospheric GCM's reproduce the Arctic pressure patterns that will produce the key features of ice motion observed in the Beaufort Gyre, transpolar drift stream, and East Greenland drift.

22.2.5 *Process Models*

In addition to the model examples given in Sections 22.2.1 through 22.2.4, a variety of other physical models exist to represent the individual components of sea ice models, including detailed thermodynamics of heat transport, turbulent flux models at the air–ocean interface, atmospheric boundary layer processes, radiative models of longwave and shortwave radiation, and simplified oceanic mixed layer models.

As noted earlier, heat transport through the snowpack is typically treated in terms of conduction only, with one average thermal conductivity used for the entire snow column (e.g., [Parkinson and Washington, 1979; Semtner, 1976; Maykut, 1982]). Colbeck [1991] discusses some of the approaches used to address conduction as well as turbulent fluxes through homogeneous and layered snowpacks. Penetration of the snowpack at optical wavelengths is assumed to be negligible [Parkinson and Washington, 1979], or treated with a single transmittance value (e.g., [Gabison, 1987] and Section 22.2.1). More detailed treatments of thermal and radiative properties of the snowpack are described by Weller and Schwerdtfeger [1977] and Schwerdtfeger and Weller [1977]. Turbulent fluxes at the snow/ice–air surface and open-water–air surface are treated simplistically in three-dimensional ice models, with a single energy transfer coefficient for a variety of different surface types. Andreas and Murphy [1986], Andreas [1987], Morris [1989], and Smith et al. [1990] discuss more detailed treatments of turbulent transfer over ice surfaces and leads. Specific processes of ice growth and oceanic modifications in refreezing leads are discussed by Bauer and Martin [1983] and Kozo [1983].

In addition to the treatments of atmosphere–ocean–ice coupling presented earlier, simplified models exist with the potential to improve the performance of the existing ice models. Overland et al. [1983], Chu [1987], and Overland [1988] describe models of the atmospheric boundary layer over the ice pack. A simplified coupling of the ice cover to the boundary layer is described by Koch [1988]. Simple representations of the upper ocean applicable to ice modeling are described by Fichefet and Gaspar [1988] and Wood and Mysak [1989]. A variety of parameterizations to improve the accuracy of the longwave and shortwave fluxes that are input to the ice models are available, ranging from simplified approaches [Harvey, 1988; Shine and Henderson-Sellers, 1985; Ebert and Curry, 1990] to more complete transmittance models [Kneizys et al., 1988].

22.2.6 *Model Parameterizations of Fields Available From Satellite Data*

The previous section contained a summary of the types of numerical models that presently exist to describe the interaction of atmosphere, ice, and ocean. In order to better clarify the relationship between these numerical models and remotely sensed data, the following description of existing parameterizations of key model fields is presented.

In particular, the fields that are or will soon be available operationally from satellite data are ice extent, concentration, multiyear fraction, and velocity.

Ice extent is determined in a relatively straightforward manner from models containing sea ice thermodynamics and/or dynamics. When the temperature of the mixed layer (or upper layer of the ocean) falls below freezing (approximately −1.8°C) in a particular grid cell, sea ice forms in that grid cell. The ice is subsequently advected into other grid cells or it remains in its area of formation; melt may occur at any time. Ice extent can be defined as the equatorward limit of sea ice (of any concentration). Alternatively, ice extent is often expressed quantitatively as the ocean area poleward of this limit or, e.g., in the NASA sea ice atlases [Zwally et al., 1983; Parkinson et al., 1987] as the area with ice of concentration ≥15%. The areal summation is performed similarly whether one is evaluating ice extent from observational (satellite) data or from model output. Slight discrepancies may be introduced by the spatial resolution of the data or model output from which ice extent is evaluated.

Ice concentration, which provides direct information on the open water fractions within an area of sea ice, can change by several mechanisms in model simulations: advection, divergence or convergence, and freezing or melt. Small changes of ice concentration can also be caused by diffusion terms, which are included in some models in order to mimic the effects of subgrid-scale motions or to provide numerical stability. Melt can affect ice concentrations by changing the thickness (to zero) or by melting the ice laterally (e.g., in leads). In models containing only a single ice thickness, melting at the surface can change the concentration without melting all the ice in a grid cell if the single thickness is assumed to represent the mean of a range of thicknesses, e.g., a linear distribution of thicknesses between zero and twice the mean (e.g., [Hibler, 1979]). This strategy has not been adopted in GCM's, but it has been used in various stand-alone ice models [Preller and Posey, 1989; Walsh and Zwally, 1990]. Changes of ice concentration by freezing, on the other hand, are typically assumed to create ice of a uniform thickness over all open water in a grid cell unless the model formulation includes a prescribed minimum fraction of leads or open water.

The formulation of the multiyear ice fraction is based partially on the definition of multiyear ice: sea ice that has survived at least one summer's melt season. Consequently, models that carry multiyear ice as a variable impose an abrupt transition from first-year ice to multiyear ice. This transition can occur either at the time when the mixed layer temperature drops to freezing or at a prescribed date (e.g., September 1 in the Arctic). When multiyear ice is present, its concentration changes by the same processes that change total ice concentration: advection, convergence or divergence, diffusion, and melting. (Multiyear ice, by definition, cannot form instantaneously by freezing.) Surface heat budgets are computed separately for the first-year and multiyear ice within a grid cell. The ice rheology determines the extent to which convergence deforms first-year and multiyear ice. According to present algorithms [Walsh and Zwally, 1990], convergence deforms solely first-year ice as long as the concentration of first-year ice exceeds 5%. The formulation of the ice strength, which has been made a rather ad hoc function of the amounts of first-year and multiyear ice, needs further attention in models that distinguish several types of ice. Hibler's [1980a] multiple-thickness formulation provides a possible point of departure for formulations of the strength of first-year and multiyear ice mixtures.

22.3 MODEL REQUIREMENTS OF SATELLITE DATA

Ice–ocean models require observational data for their initialization and validation. Moreover, the use of observational data for the forcing of ice–ocean models provides an objective means for model testing and assessment when the models are run in a decoupled (from the atmosphere) mode. The general lack of in-situ measurements from ice-covered waters makes satellite remote sensing the cornerstone of data assimilation schemes required for ice modeling.

The manner in which data are used for model initialization depends on which of three types of ice model simulation is being performed: short term (days), long term with periodic forcing, and long term with aperiodic forcing. An example of short-term simulation is the use of an operational model to forecast sea ice at ranges of several days (e.g., PIPS). For such simulations, an accurate initialization corresponding to the actual sea ice state is crucial to the success of the forecast. The second type of model integration, a long-term periodic simulation, spans at least several years with an annual cycle of forcing that repeats itself exactly. In such cases, the ice model should achieve equilibrium if run for a sufficiently long time. This type of simulation is useful for diagnostic studies of the ice–ocean system (e.g., [Hibler and Bryan, 1987; Semtner, 1987]) and for assuring that the ice model is free of long-term biases or model drift prior to interactive coupling (such as to an atmospheric GCM). Provided that sufficient computational resources are available, a realistic initialization is not essential for such simulations because the model should eventually achieve equilibrium with its forcing. The third type of simulation, the long-term aperiodic run, is used to obtain an interannually varying history tape of the sea ice state. Examples include the hindcast simulations of Rothrock and Thomas [1990], Walsh and Zwally [1990], and Riedlinger and Preller [1991]. As in the periodic simulations described above, the model can be spun up to the initial state of the desired date by integrating (periodically or aperiodically) through several annual cycles. For this reason and because the long-term statistics of the simulation are of primary interest, a precise initial state is not essential to the success of the simulation. Nevertheless, the initial state must conform reasonably closely to the corresponding actual state if the first several years are not to contaminate the verification statistics. Thus, the spin-up of such a simulation must be achieved in such a way that it

ensures temporal homogeneity in the history tape's correspondence to observations. One may argue that the initialization strategy involves more subtleties in this type of simulation than in the other two.

The initialization and validation of ice models require observational data on several key sea ice variables: concentration, thickness and ice type, drift velocity and associated kinematic quantities, and surface properties (albedo, snow cover, temperature, etc.). While other properties such as ice salinity and temperature profiles may be important for diagnostic studies with ice–ocean models, we will focus primarily on the four variables listed above. These properties are also variables for which satellites provide useful information.

22.3.1 *Key Variables Used for Model Initialization and Validation*

22.3.1.1. Ice concentration. Ice concentration data implicitly include information on several quantities that are of central importance to studies of the large-scale distribution and variability of sea ice: fractional coverage of an area (ideally within different ice thickness ranges), ice extent, and the fraction of open water (e.g., leads) within the pack. For forecasting purposes, ice extent may be the primary concern. For coupled model studies of the Arctic or Antarctic surface energy balance, the lead fraction may be a primary concern because the small areas of leads and open water effectively govern the exchanges of heat and moisture between a pack-ice surface and the atmosphere. Different sensors provide the optimal information on ice concentration, extent, and lead fractions.

The most useful and homogeneous source of ice concentration data for large (50 km x 50 km) areas is the passive microwave data from polar orbiting satellites: the Electrically Scanning Microwave Radiometer (ESMR), the Special Sensor Microwave Imager (SSM/I), and the Scanning Multichannel Microwave Radiometer (SMMR). Since 1978, these satellites have provided nearly continuous coverage at 1- to 2-day intervals and 50-km resolution with more scattered coverage being available since 1972. The recent availability of gridded passive microwave data on CD-ROM (through the National Snow and Ice Data Center) has greatly facilitated the use of derived ice concentrations by the sea ice community.

The accuracy of any data used for model verification or data assimilation is a key consideration in determining its usefulness. Errors in the total ice concentration (first-year plus multiyear ice) and ice edge location as derived from passive microwave data are fully discussed in Chapters 4, 10, and 11. The estimated errors for total ice concentration generally range from 5% [Cavalieri et al., 1984; Swift and Cavalieri, 1985; Steffen and Maslanik, 1988] to about 15% [Steffen and Schweiger, 1990] using general versions of the NASA Team algorithm, with errors as low as 3% when the algorithm is tuned for local conditions. Absolute accuracies remain uncertain and somewhat controversial due to the difficulties of comparing different data types and different scales. Total ice concentration estimates are relatively unaffected by surface melt on a regional basis, except when melt ponds are present (e.g., [Steffen and Maslanik, 1988]). Gloersen and Campbell [1988] describe some more specific effects of surface melt on retrievals of ice concentration and ice type. In addition to melt effects, sources of error include the effect of surface wind on open water, atmospheric water content, changes in the ice surface (snowpack, flooding, etc.), and the presence of radiometrically thin ice not accounted for by the algorithm.

For broad depictions of the total ice concentration fields in large-scale models (with resolutions on the order of 100 km), the accuracy and resolution of the passive microwave data are certainly adequate, except perhaps during late summer when substantial melt ponding is present. However, mesoscale models may require finer resolution and greater accuracy (for the determination of the location of leads and polynas in the pack) for initialization and validation at the 10-km scale.

The concentrations derived from satellite passive microwave data provide part of the input to the Navy and National Oceanic and Atmospheric Administration (NOAA) Joint Ice Center's (JIC) weekly analyses, which have been used in the initialization of the PIPS model and in the compilation of verification statistics from long-term simulations [Walsh et al., 1985]. The JIC depictions of the ice edge have also utilized information from the radar altimeter on the Geosat satellite. Because the shape of a radar altimeter's return pulse is significantly different over sea ice and open water, the altimeter permits the resolution of the ice edge to within 10 km, which is finer than the resolution of the digitized JIC ice charts and considerably finer than the resolution of the passive microwave concentration grids. For simulations with mesoscale models, radar altimeter data can serve a useful purpose in the initialization and validation of the ice edge.

Fine resolution imagery is needed to resolve the individual small areas of open water (leads and polynas) within the pack ice. Together with areas of thin ice, these open water areas are the primary determinants of the ice strength, the ocean–atmosphere heat exchange, and the evaporation from the ocean. Because the open water areas often have scales of tens to hundreds of meters, individual open water areas cannot be resolved by current passive microwave satellite imagery, although such subresolution features are included in the total open water area within the passive microwave field of view. Moreover, the uncertainties of several percent in the passive-microwave-derived concentrations are comparable to the variations in the small percentages of thin ice and open water that typically occur in pack ice (e.g., [Maykut, 1982]). Both visible and infrared imagery can provide fine-resolution (10 meters to 1 kilometer) observations of ice concentration, ice extent, lead locations, and floe characteristics. Visible and reflected infrared imagery are limited, however, by both clouds and darkness while thermal infrared imagery is limited by

cloud cover. The most promising source of all-weather, fine-resolution data is the satellite-borne Synthetic Aperture Radar such as those on board ERS-1 (from which data are currently becoming available), JERS-1, and Radarsat. Nominal resolution from the JERS-1 SAR, for example, will be 30 m.

The accuracy of ice concentration from SAR data is discussed in Chapter 6. Generally, errors in SAR-derived ice concentration occur primarily when thin ice is present, since thin ice can have backscatter characteristics similar to that of open water. However, a comparison of ice concentrations calculated from visible-band aerial photographs, passive microwave acquired from aircraft, and SAR generally agreed to within 15%, with ice–water contrast and ice signature variability accounting for the error [Burns et al., 1987].

Considerable potential exists for the use of SAR data in model parameterization studies directed at the realistic simulation of the thin ice and open water areas within pack ice. Mesoscale models, in particular, will benefit from the order of magnitude improvement in resolution made possible by SAR. In addition to uses by the ongoing ice modeling efforts summarized here, such information may serve as a stimulus to the coupling of sea ice and atmospheric models through realistic parameterizations of surface–atmosphere heat exchange.

One additional use of satellite-derived ice concentrations is the specification of lead fractions in climatic models as noted in Section 22.2.4. In the Australian global climate model [W. Budd, personal communication, 1991] for example, the specified lead fractions are the seasonally varying fractions of open water derived from the microwave radiances of the ESMR and SMMR instruments.

22.3.1.2. Ice thickness and ice type. The spatial and temporal variations of ice thickness are notoriously difficult to quantify. The only data on sea ice thickness have been obtained from: (1) holes drilled through the ice, a logistically difficult and expensive procedure; (2) submarine sonar data, much of which is classified, providing snapshots for single year-months along specific cruise tracks; and (3) single-point time series obtained from moored acoustic sensors, which have come into use only during the last few years. Sources (1) and (2) have permitted the computation of a seasonal climatology of Arctic ice thickness (e.g., [Bourke and McLaren, 1992]) used to validate ice models in a general way, but they have provided little information on interannual variability.

There are no immediate prospects for the direct measurement of ice thickness by satellite, although relationships between ice thickness and passive microwave polarization ratios have been demonstrated (e.g., [Steffen and Maslanik, 1988]). The estimates of multiyear ice concentration obtained from passive microwave data can provide crude and quantitative indicators of ice thickness, but such indicators are inadequate for model initialization and verification. Thus, there will most likely be a continued reliance on the fragmentary thickness measurements obtained from the surface and subsurface sources.

Several models explicitly include the concentration and thickness of multiyear ice in their formulation [Rothrock and Thomas, 1990; Walsh and Zwally, 1990]. The results of the latter model show some agreement with the interannual fields of multiyear ice concentration derived from SMMR. However, uncertainties in the SMMR-derived concentrations of multiyear ice are substantial, and useful information on multiyear ice cannot be obtained during the spring and summer months due to changes in the dielectric properties of the ice pack with the onset of melt (see Chapter 4). During winter, average accuracy for ice type has been estimated to be within about 20% [Cavalieri et al., 1984], although the error may be considerably larger even in winter [Comiso, 1986]. For these reasons, the Kalman filter approach of Rothrock and Thomas provides an attractive means for assimilating the limited satellite data into a more temporally homogeneous framework. This framework offers the potential for a more meaningful validation of the time-varying fields of multiyear ice coverage (and ice thickness) simulated by the more traditional sea ice models.

22.3.1.3. Ice velocity and associated kinematic variables. Because ice velocity has a relatively short time scale (days), accurate initialization of ice motion is important primarily for short-term simulations. For long-term simulations, however, the mean patterns of ice drift determine the transports of mass and salinity. The validation of the simulated drift is therefore an important element of model simulations of long periods (seasons or longer).

The primary source of data on time-varying ice velocities has been the collection of position measurements of Arctic buoys and drift stations. The buoy data have been objectively analyzed on a daily basis since 1979 by the University of Washington's Polar Science Center. These velocities have been used to verify model simulations of ice velocity (e.g., [Serreze et al., 1989]). The satellite passive microwave data, although way too coarse in resolution to identify individual ice floes, nonetheless permit the derivation of approximate, generalized velocity vectors on the basis of changes of multiyear ice concentration over periods of several months to a season. Such derivations are based on the supposition that multiyear ice behaves somewhat like a tracer in subfreezing regions poleward of the ice edge. For example, velocities derived from changes of the position of the multiyear ice edge have been found to be spatially coherent, interannually variable, and consistent with the fields derived from a sea ice model [Zwally and Walsh, 1987].

The most promising source of information on individual floe ice velocities is SAR imagery as discussed in Chapter 18. Pattern recognition techniques can be applied to SAR images of the same region at intervals of several days, thereby providing kinematic vector images of the net ice motion during the intervening time period (e.g., [Curlander et al., 1985]). Emery et al. [1991] used a similar approach

with Advanced Very High Resolution Radiometer (AVHRR) data to obtain ice velocity vectors for the Fram Strait region; these vectors were compared directly with model-derived ice velocities. The use of data in this manner is likely to provide the most precise means of initializing and validating ice velocities from mesoscale models and, perhaps, also of validating the integrated measure of the divergence and convergence over grid cell areas of larger scale models. It should be noted in this regard that the time differences of multiyear ice concentrations derived from satellite passive microwave data also provide potentially useful information on sea ice convergence and divergence over larger areas (hundreds of kilometers), as discussed in Section 22.4.2.

22.3.2 Additional Satellite Data for Future Use in Models

22.3.2.1. Albedo and ice surface temperature. One of the critical thermodynamic properties in a sea ice model simulation is the surface albedo. While the albedo's broad dependencies on the surface state (snow, bare ice, and puddled ice) are generally known, the spatial and temporal variations of surface albedo in ice-covered regions are poorly documented. In view of the high leverage of the surface albedo, especially in sea ice simulations that address climate change, the parameterization and validation of surface albedo merit increased attention.

Albedos over ice cover, on scales suitable for model input, have been both mapped from digital AVHRR imagery (e.g., [Rossow et al., 1989]) for short time periods and interpreted from Defense Meteorological Satellite Program (DMSP) Operational Line-Scan System (OLS) transparencies [Robinson et al., 1986; Scharfen et al., 1987] for about a ten-year period. These DMSP albedos were tested in an ice model by Ross and Walsh [1987]. Robinson et al.'s results cover only the central Arctic during the summer melt season (May through August), but do provide quantitative depictions of the interannual variations over areas of 1000 km x 1000 km. Unfortunately, the variation of regional surface albedo is intertwined with the distribution of open water within the region. Model biases regarding open water fractions may overwhelm the effects of variation in the snow–ice surface albedo. A need therefore exists for a more complete utilization of high-resolution satellite imagery to address the validity of model treatments of surface albedo within a grid cell. It is likely that combined usage of SAR and high-resolution visible imagery will be required for a meaningful assessment of the parametric needs relative to surface albedo.

The energy balance calculations necessary to estimate ice surface temperature for ice growth and decay in models are substantial sources of uncertainty. Direct measurement of ice surface temperatures would be particularly valuable for ice prediction models. Comiso [1983] used data from the temperature-humidity infrared radiometer (THIR) on board Nimbus 7 to estimate ice surface temperatures covering nine months in the Arctic. Schluessel and Grassl [1990] describe the use of AVHRR to retrieve water and ice surface temperatures in Antarctic polynyas. Key and Barry [1989] describe the retrieval of ice surface temperatures and albedos for a portion of the Arctic using AVHRR imagery. An example of the calculation of ice albedos and temperatures from AVHRR for operational ice forecasting is discussed by Condal and Le [1984]. With the exception of the albedos mapped from DMSP OLS data, no albedo or temperature data set has been prepared for the Arctic that covers more than several months. Henderson-Sellers and Wilson [1983] review some older albedo climatologies suitable for model input. Work is underway to refine the methodology to map ice surface temperatures (as well as cloud cover) from AVHRR as part of the Earth Observing System Polar Exchange at the Sea Surface (POLES) program.

22.3.2.2. Snow cover. Snow cover is clearly a key element of the albedo formulation discussed above. Snow depth also affects the wintertime energy budget over sea ice. While snowfall is an externally prescribed quantity in the context of ice modeling, there is nevertheless a need for more information on the distribution of snow depth within the grid-cell areas of models. The extent to which altimeters and/or SAR can provide such data is unclear. Attempts to use passive microwave (SMMR) data to estimate snow depth over land have, however, met with some success for specific regions [Chang et al., 1987]. A discussion of the use of passive microwave data to determine snow depths over sea ice is presented in Chapter 16. Advances in studies of snow depth in regions covered by sea ice are needed to permit modelers to determine whether biases in simulated sea ice (e.g., thickness) can be attributed to biases in the prescribed snowfall or snow depth.

22.3.2.3. Sea surface temperature. Sea surface temperatures suitable for ice modeling have been available for several years and are derived from ship observations (e.g., the comprehemsive ocean-atmosphere data set, COADS) and satellite imagery such as AVHRR, including the operational generation of sea surface temperatures by NOAA/NESDIS (National Environmental Satellite, Data and Information Service), the multichannel sea surface temperature fields (e.g., [McClain et al., 1985; Barton, 1985]) and from sounder data (e.g., [Susskind and Reuter, 1985]). Minnett [1990] reviewed some of the attributes of sea surface temperatures measured from space, including the problem of determining skin versus bulk temperatures (e.g., [Schluessel et al., 1987; Schluessel and Grassl, 1990]). While the noise level of individual temperature measurements from AVHRR is about 0.1 K, the unmodeled effects of the intervening atmosphere reduce this accuracy. The Along-Track Scanning Radiometer, carried on board ERS-1, is designed with both a lower noise level, as well as the ability to observe two paths through the atmosphere, to achieve more precise and accurate surface temperatures.

22.3.2.4. Cloud cover. Parameterizations of radiative fluxes in ice models can benefit from reliable cloud cover

observations. Long-term cloud cover statistics derived from satellite data for the polar regions include the three-dimensional nephanalysis carried out by the U.S. Air Force [Fye, 1978; Tian and Curry, 1989], the International Satellite Cloud Climatology Program (ISCCP) [Rossow et al., 1985; Rossow and Schiffer, 1991], and analyses of THIR imagery [Stowe et al., 1988]. Henderson–Sellers [1984] describes some of these climatologies, as well as cloud climatologies, from surface observations. Some of the problems of comparing cloud climatologies based on satellite data versus surface observations are reviewed by Henderson–Sellers and McGuffie [1990], and different satellite-derived cloud statistics for the Arctic are discussed by McGuffie et al. [1988]. Serreze and Rehder [1990] describe a climatology for June spanning 12 years of DMSP interpretations for the western Arctic. Barry et al. [1987] give DMSP-derived cloud statistics for the Arctic for April through June 1979 and 1980. Key and Barry [1989] and Ebert [1989] describe some of the problems of automated mapping of polar clouds and AVHRR-based cloud mapping schemes designed specifically for the polar regions.

Outgoing longwave radiation fluxes are available directly from AVHRR data [Gruber and Jacobowitz, 1985], High-Resolution Infrared Radiation Sounder data [Ellingson et al., 1989], and the broadband channels of the Earth Radiation Budget Experiments (ERBE) (e.g., [Kopia, 1986; Jacobowitz et al., 1984; Barkstrom and Smith, 1986; Ramanathan et al., 1989]). Relatively long time series of these data are available at different spatial and temporal scales for the polar regions.

22.3.2.5. Atmospheric properties. Atmospheric properties (water vapor, liquid water, and temperatures) are determined operationally using sounders as well as passive microwave imagery. Sounders provide information on the vertical distribution of atmospheric conditions, while passive microwave images provide integrated values for water content. Calculations are complicated over ice and snow due to the high and variable emissivity of the surface.

Surface air temperatures used in ice model simulations are generally prescribed, either from objective analyses of station data or from atmospheric model output. The effects of errors and biases in these temperatures need assessment in much the same way as do the effects of errors in the albedo and snow depth as discussed above. The use of satellite data for such assessments does not appear to have been fully exploited, although the products of the ERBE and ISCCP efforts may be useful in this regard.

Finally, wind speed over open ocean is routinely determined from passive microwave imagery and can be mapped from SAR data. Speed and direction can be measured by scatterometers. Over sea ice, no direct way of measuring surface winds from satellites is available, although cloud motions have been used to map upper-level winds over polar regions [Turner and Warren, 1989].

22.4 EXAMPLES OF THE INTERACTION OF MODELS WITH DATA

22.4.1 Model-to-Data Comparison Studies

Comparisons with satellite data have provided one of the major vehicles for recent assessments of sea-ice model performance. As discussed below, some model results have provided insights to the validity of satellite-derived fields of variables that are only indirectly measurable.

Comparisons between model output and satellite data generally require systematic compilations of satellite measurements of one or more of the variables simulated by a model. An outstanding example of such a compilation is the record of the sea ice extent and concentration derived from satellite passive microwave measurements (ESMR, SMMR, and SSM/I). The passive microwave data are also a primary input to the JIC's weekly ice charts, which have been used for a host of additional model-to-data comparisons. The availability of the passive microwave grids of ice concentration from 1973 onward provides a climatology as well as a 15- to 18-year sample of interannual fluctuations about the seasonal means.

Among the first model studies to have utilized data on ice extent derived from passive microwave imagery were those of Parkinson and Herman [1980] and Lemke et al. [1980]. In the latter study, a stochastic-dynamic model was calibrated using 10 years of monthly data on ice extent. Subsequently, the satellite-derived fields of ice extent have been used by Hibler and Walsh [1982], Hibler and Ackley [1983], Parkinson and Bindschadler [1984], Walsh et al. [1985], Preller [1985], Hibler and Bryan [1987], Semtner [1987], Stossel et al. [1989], Fleming and Semtner [1991], and Walsh and Chapman [1991]. Satellite-derived ice concentrations in the vicinity of the Weddell polynya stimulated the modeling studies of Martinson et al. [1981], Parkinson [1983], and Motoi et al. [1987].

While most model-to-data comparisons of ice extent have been intended to assess the climatologies simulated by models, several studies have used satellite-derived data to evaluate the ability of models to reproduce interannual fluctuations of ice cover. Walsh et al. [1985], for example, found that the Hibler [1979] two-level model reproduced approximately 50% of the year-to-year variance of ice coverage in 20 longitudinal sectors of the Arctic. Walsh and coworkers used interannually varying winds and air temperatures, but climatological ocean forcing to drive a stand-alone sea ice model. Fleming and Semtner [1991] subsequently showed that the verification statistics are improved somewhat when the ice model is coupled to an interactive ocean model.

More specific use of the ice concentrations derived from passive microwave measurements has been made by Serreze et al. [1990], who used an ice model and other tools to diagnose the origins of a large area of reduced ice concentrations within the Arctic pack ice during 1988. Serreze and coworkers supplemented the passive microwave data with visible-band imagery during the sunlit season.

Additional uses of satellite measurements for model-to-data comparisons have been made by Walsh and Zwally [1990], whose application of satellite-derived multiyear ice concentrations is discussed in Section 22.4.2, and by Emery et al. [1991], who used AVHRR imagery to obtain ice velocity vectors for the region east of Greenland. In the latter study, discrepancies between model- and satellite-derived velocities indicated that the strength of an ocean current had been underspecified in the model forcing. Ross and Walsh [1987] compared interannual fluctuations of Arctic Ocean surface albedo with those derived from satellite imagery by Scharfen et al. [1987].

22.4.2 *Hindcast Studies: Walsh and Zwally [1990]*

Hindcast studies of the interannual fluctuations of sea ice have been performed by using observational analyses of atmospheric forcing variables (air temperatures and pressure-derived winds) to drive the Hibler two-level model over time scales of several years to several decades [Walsh et al., 1985; Walsh and Zwally, 1990]. The inclusion of multiyear ice in the simulations was motivated by the availability of the multiyear ice concentrations derived from satellite passive microwave measurements. The oceanic component of the model consisted of only a constant-depth mixed layer and time-independent currents. The currents were obtained geostrophically from a prescribed dynamic topography.

As noted in the previous subsection, runs of the model in this mode explain about 50% of the interannual variability of satellite-derived coverage of total sea ice (first-year plus multiyear ice). The simulated values of multiyear ice concentration are generally larger than those derived from the SMMR data. Although several arbitrary elements of the model formulation may contribute to this discrepancy, Comiso [1990] has recently reported that SMMR-derived multiyear concentrations from the SMMR Team algorithm are also smaller than one would infer from the concentrations of ice surviving the summer melt in the Arctic. The interannual variations of SMMR- and model-derived multiyear ice coverage generally show somewhat ambiguous agreement in the Arctic Ocean (Figure 22-2).

The SMMR data also permit the estimation of generalized resultant velocity vectors on the basis of changes in the multiyear ice edge over periods of several weeks to a season. Such estimations are limited to the nonsummer months, when surface wetness does not contaminate the multiyear ice signature.

Instances of convergence/divergence in the numerical model results have been confirmed by corresponding changes in the multiyear ice concentrations derived from the SMMR data, although the model-derived changes are smaller than those obtained from SMMR. Larger samples of such comparisons, including buoy-derived velocity divergences, are needed to determine whether there is a bias in either the SMMR or the model depictions of short-term divergence events. The outcome of such comparisons has important implications for the validity of the simulated mass budget, since most of the ice growth in the central Arctic occurs in areas of thin ice or open water (e.g., leads) that result from divergence of pack ice.

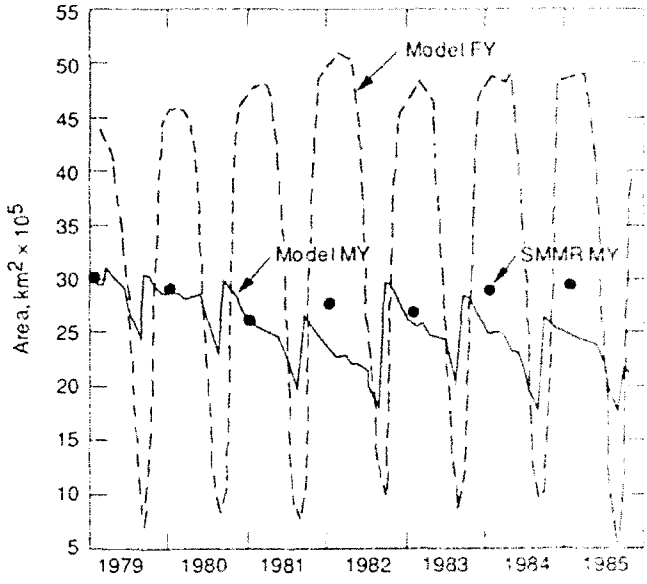

Fig. 22-2. Time series of model-derived multiyear and first-year ice coverage in the Arctic. Also shown are November–April averages from SMMR data, adjusted to include an estimated 8.2×10^5 km^2 in the unobserved area north of 84° N [Walsh and Zwally, 1990].

22.4.3 *The Use of Models With Data in Forecasting*

The Polar Ice Prediction System is a sea-ice forecasting system based on the Hibler ice model [Preller, 1985; Preller and Posey, 1989]. It is used for the daily prediction of ice drift, ice thickness, and ice concentration in the Arctic by the U.S. Navy (Figure 22-3). In this system, the Hibler ice model is driven by daily atmospheric stresses and heat fluxes from the Navy Operational Global Atmospheric Prediction System and by monthly mean ocean currents and heat fluxes derived from the Hibler and Bryan [1987] ice–ocean model. The model is run in an operational environment at the Fleet Numerical Oceanography Center (FNOC). A 120-hour forecast of several different ice fields is produced daily. Each day's forecast is initialized from the previous day's 24-hour forecast (Figure 22-4). Once each week, the model's ice concentration field is initialized from a digitized field of observed ice concentration made available by the Navy/NOAA Joint Ice Center (Figure 22-5). This field is a subjective analysis derived from multiple data sources [Wohl, 1991]. Satellite data used in the analysis come from the AVHRR, visible data from the DMSP OLS, and passive microwave data from the SSM/I. In addition to these satellite data, any available ice reconnaissance flights or ship observations are blended into the weekly analysis.

During model initialization, the observed ice concentration totally replaces the modeled ice concentration from the

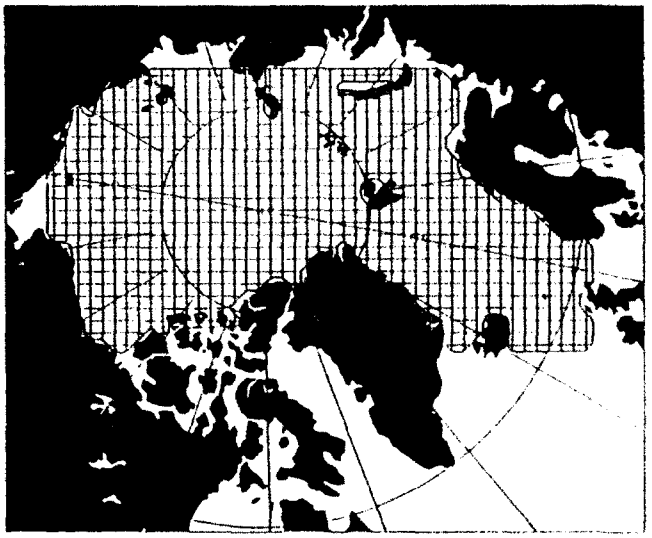

Fig. 22-3. Model domain and grid used by PIPS. Grid resolution is 127 km.

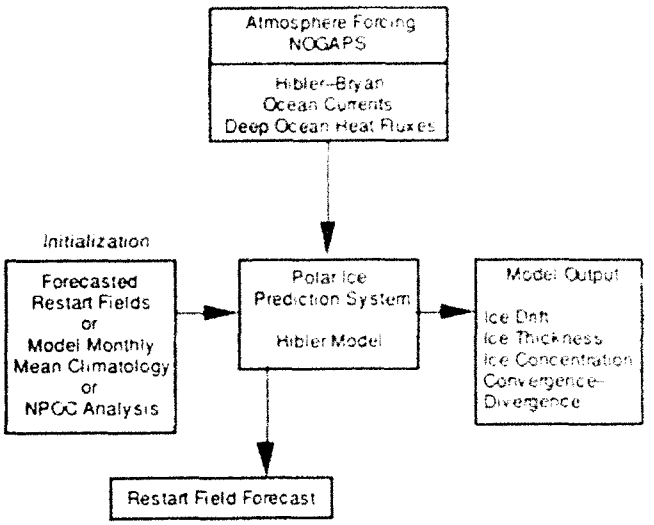

Fig. 22-4. The design of PIPS

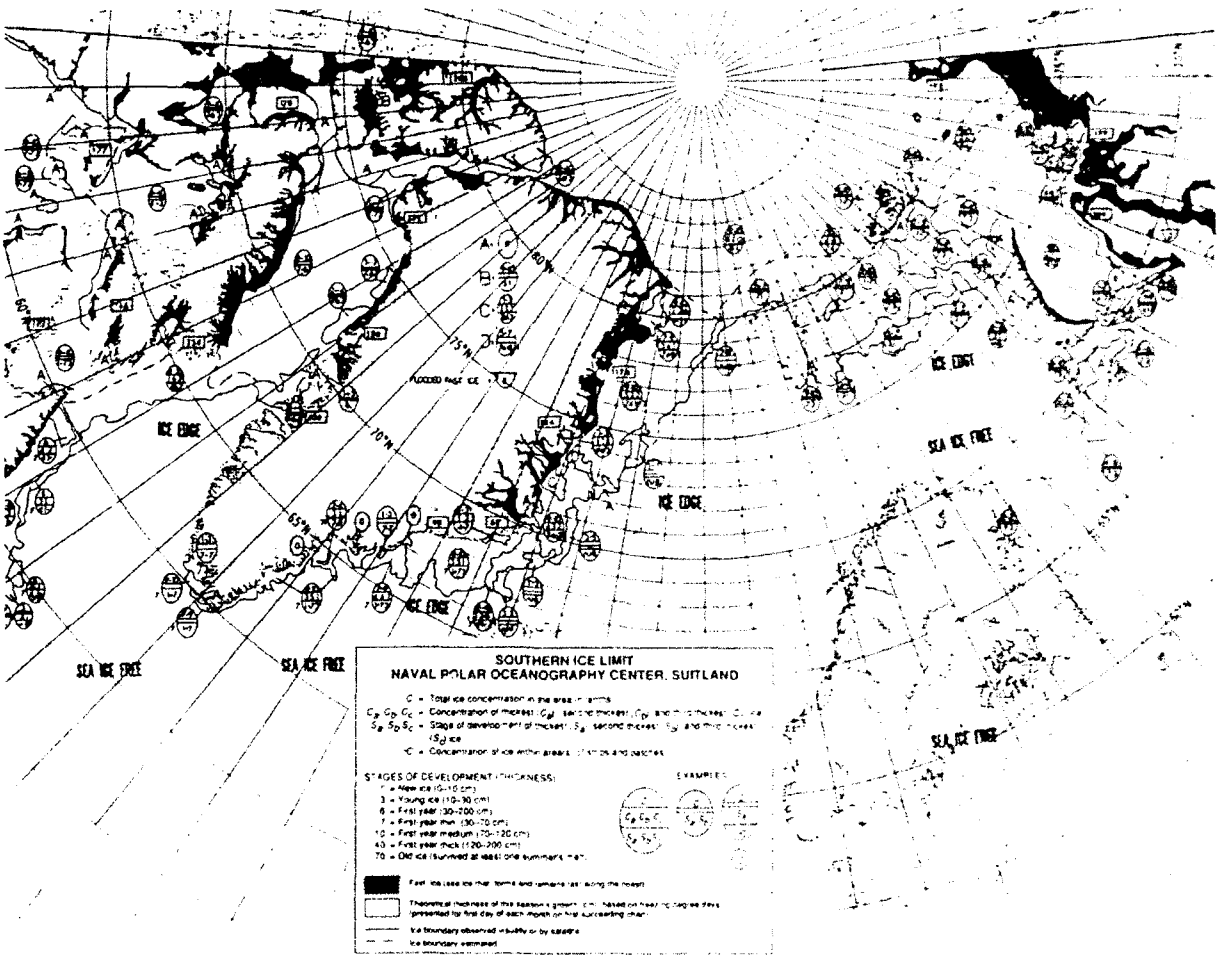

g. 22-5. Navy/NOAA Joint Ice Center weekly analysis of sea ice concentration for the eastern Arctic for June 5, 1991

previous day's 24-hour forecast. Other variables from the previous day's forecast remain unchanged, with the exception of the ice thickness and the heat stored in the ocean's mixed layer. These fields are adjusted only near the ice edge to be consistent with the ice edge defined by the JIC data as shown in Figures 22-6(a) and (b). This adjustment involves removing ice from regions that should not be ice covered and adding heat to the mixed layer by raising its temperature. If the model forecasts no ice in a region where the data indicate it should exist, heat is removed from the mixed layer by setting the temperature back to freezing and either 0.5 or 1.0 m of ice is added to that grid cell depending on the observed concentration [Preller and Posey, 1989]. Two similarly designed forecast systems, the Regional Polar Ice Prediction System Barents Sea (RPIPS-B) and the Regional Polar Ice Prediction System Greenland Sea (RPIPS-G) forecast over the Barents and Greenland Seas at a higher resolution than PIPS [Preller et al., 1989].

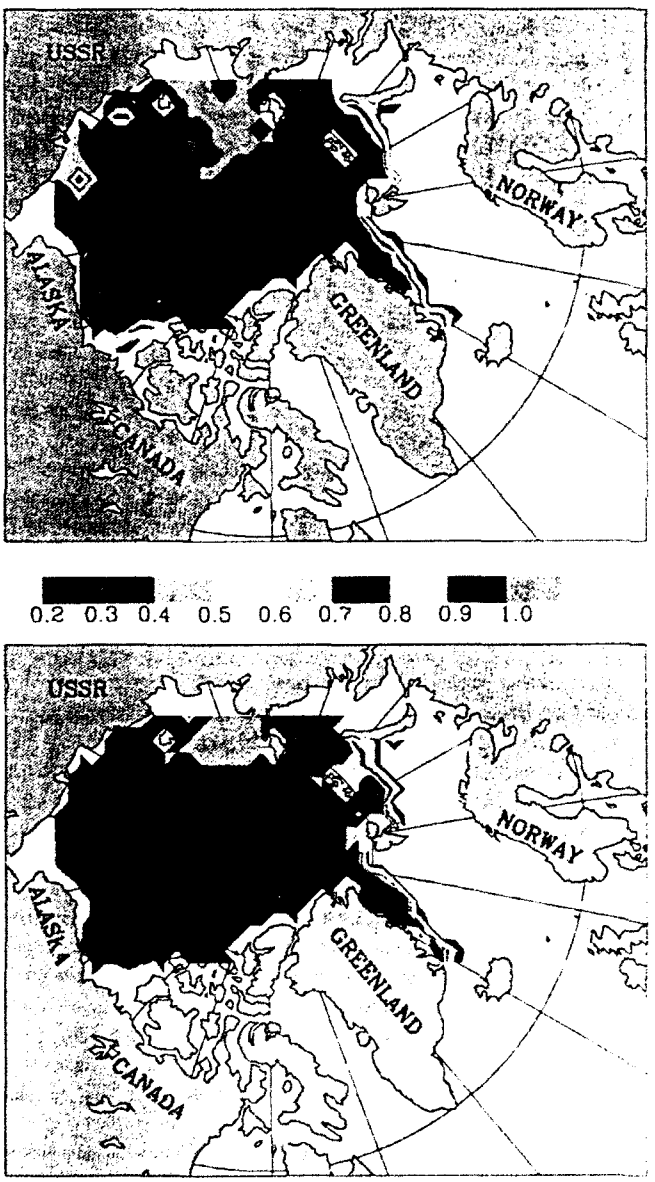

Fig. 22-6. PIPS 24-hour forecast ice concentration from (a) June 6, 1991, and (b) June 7, 1991, immediately following the initialization of PIPS by the JIC analysis. (The USSR is now referred to as the Commonwealth of Independent States.)

Data assimilation and model initialization in an operational forecasting system are dependent on a number of different factors. Availability of the data is the first important factor. The data must be available to the computer system used by the forecast model.

The second factor is the age of the data. The model uses data to provide the most realistic initial state for the forecast. If the data are old, they can provide incorrect information to the model. The JIC completes its analysis each Thursday; the analysis is ready for use in PIPS by the end of the day on Friday. The two-day lag in JIC data is not optimal, but is considered acceptable in the PIPS model. PIPS uses a resolution of 127 km. The ice edge, on average, does not move more than 100 km over 48 hours, so the observed changes may not be resolved by the model. There are certainly exceptions, such as the appearance of the Odden over a 24-hour period or the rapid movement of the ice edge brought about by extremes in the atmospheric forcing (strong winds). A 48-hour time delay in the data can, however, be a problem in the RPIPS-B and RPIPS-G models. Since these models use resolutions of 20 and 25 km, respectively, movement of the ice edge in these regions can be a grid distance or more over a 48-hour period. Ideally, the *data used for initialization should be no more* than 24 hours old. The importance of the age of the data also implies that data assimilation techniques such as Kalman filtering, which fits a time series of data into a predictive model, may not provide the most recent ice conditions for initializing a forecast. Also, the Kalman filter may not be the optimal choice in an operational system where computer time is limited (the Kalman filter is computer intensive) and where historical data are not often saved and available for use with the filter.

The third important factor is the frequency of the data. The JIC analysis is available only once per week. However, FNOC now has a digitized data set of ice concentration from the SSM/I available in real time each day (Figure 22-7). That data set is presently being tested as an initialization field for PIPS on those days that the JIC analysis is unavailable.

In addition, Cheng and Preller [personal communication, 1991] have designed a method of blending two or more concentration fields into one maximum likelihood estimate using nonlinear regression. The technique can be described by borrowing the terminology of the physical and measurement models from Thorndike [1988] and Thomas and Rothrock [1989] (see Chapter 23). The physical model describing pack ice evolution can be written as

$$\vec{X}_j^{t+1} = H_j\left(\vec{X}_j^{t}\right) + \vec{\varepsilon}_j^{t} \qquad (9)$$

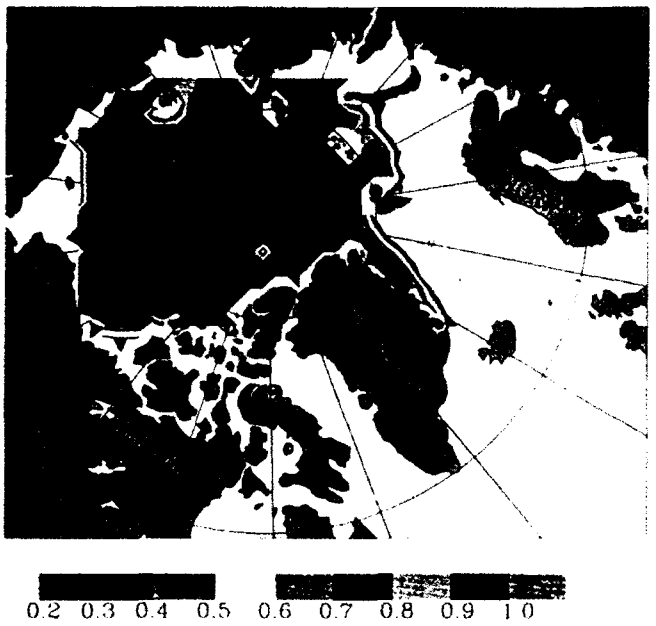

Fig. 22-7. SSM/I ice concentration from FNOC, derived using the Navy algorithm, for June 7, 1991. Values have been interpolated to and plotted on the PIPS grid.

where X is the ice concentration, H is the physical model PIPS, ε is the residual of the physical model, i and j are the spatial indices, and t is the time index. The physical model uses dynamic and thermodynamic equations along with atmospheric and oceanic forcing to predict X_j^{t+1}. The measurement model is used to update the value of X for the physical model. Written in a general form,

$$\vec{Z}_m^t = G_m\left(\vec{X}_n^t\right) = \vec{e}_m^t \qquad (10)$$

where Z represents the data (i.e., observations, measurements, constraints, and assumptions), G is the measurement model (in this case the continuity equation for ice concentration), e is the residual between the measurement and the corresponding model value, and m and n are spatial indices.

The JIC analysis and passive microwave data (other data may be included) provide field observations or measurements. The PIPS ice concentration provides a data set of historical information, while the continuity equation for ice concentration represents the constraint for these ice concentration fields. All of these data and the constraints imply that the measurement model is defined as an overdetermined problem, which is particularly suited to nonlinear regression. The method also allows for emphasizing the reliability of the data in regression by applying variable weights to the data.

Remotely sensed data have also been used for validating the Navy's operational sea-ice forecast systems. Each U.S. Navy operational model is put through an operational evaluation, lasting anywhere from three months to a year. Since 1987, an operational forecast of at least 24 hours has been made daily and archived by the Naval Research Laboratory (NRL) (formerly the Naval Oceanographic and Atmospheric Research Laboratory). These forecasts are identical to those made by FNOC and are used by NRL for continuing model verification. During the operational evaluation of PIPS, the model-derived ice edge was compared qualitatively and quantitatively to the ice edge derived by JIC. This study showed that when initialized at least once each week, the mean error in the forecast ice edge location, after seven days, was less than or equal to one grid distance. This error increased if the initialization took place less frequently [Preller and Posey, 1989].

In addition to ice edge verification, the PIPS-derived ice drift is verified against Arctic buoy data on a regular basis. Ice drift derived from the change in buoy location is statistically compared to PIPS ice drift. The result of this verification has been the continued improvement in the accuracy of the PIPS ice drift field, mainly due to improvements in the treatment of surface wind stress on the ice [Preller and Posey, 1989]. During the operational evaluation of both regional models, satellite-derived ice drift data from successive AVHRR data were used for the validation of the model-derived ice drift, Figures 22-8(a) and (b). In the case of both regional models, the direction of the modeled ice drift agreed well with the satellite-derived ice drift, however, the magnitude of the modeled drift was weaker than that derived from the satellite data.

22.5 SUMMARY AND CONCLUSIONS

Numerical models and observational data have been used together in a number of ways. Data obtained from drifting ice station, aircraft, and ship measurements collected over many years provided highly localized point measurements that were used to define many characteristics of sea ice. A more synoptic view of sea ice was obtained from the data collected in field experiments such as AIDJEX and MIZEX. These data provided the basis for an improved understanding of the dynamic and thermodynamic processes that affect sea ice. As a result, more sophisticated formulations for ice motion, including the effect of internal ice stress and the growth and decay of sea ice, have been determined and incorporated into numerical models. The models, in turn, are used to help provide insight into the accuracy of these formulations by validating the model results against observations.

Satellites have been able to provide a source of observational data both over larger areas and for longer periods of time than the more conventional field observations. A combination of fine-resolution satellite imagery, such as visible or infrared imagery, and radar altimetry, along with

coarser resolution data such as that from the passive microwave sources, have been used for verifying and validating many numerical models. A comparison of the ice edge derived from these sources with the modeled ice edge has been the favored method of model validation.

Satellite passive microwave data are particularly appealing to the large-scale models used to study interannual variability of sea ice. Passive-microwave total ice concentration has been used in the majority of model-to-data comparison studies. However, availability of multiyear ice concentration from the passive microwave data motivated Walsh and Zwally [1990] to incorporate multiyear ice into a version of the Hibler ice model. Using this formulation, they were able to show some compatibility between the interannual variations of the model- and SMMR-derived multiyear ice concentration.

A number of sources of remotely sensed data are used to create a weekly, subjective analysis of ice concentration by JIC. This analysis is used as a weekly initialization field for each of the three sea-ice forecast systems run by the U.S. Navy: PIPS, RPIPS-B, and RPIPS-G. Two upgrades are scheduled for the Navy forecast systems in the near future. The first upgrade involves the use of passive microwave data as an initialization field for the forecast systems. Passive microwave data, now available in real time from FNOC, are being tested as a data source that could provide more frequent initialization of these forecast systems. The second upgrade involves the replacement of PIPS with the PIPS 2.0 model. PIPS 2.0 will provide ice forecasts for most of the ice-covered regions in the Northern Hemisphere on a half-degree grid (Figure 22-9). The design of this system will be similar to that of PIPS, but will include a fully coupled ice–ocean model. Along with the JIC analysis, the SSM/I ice concentration will provide real-time initialization data over the entire model domain.

In addition to the passive microwave data, the recent launch of the ERS-1 satellite is now providing fine-resolu-

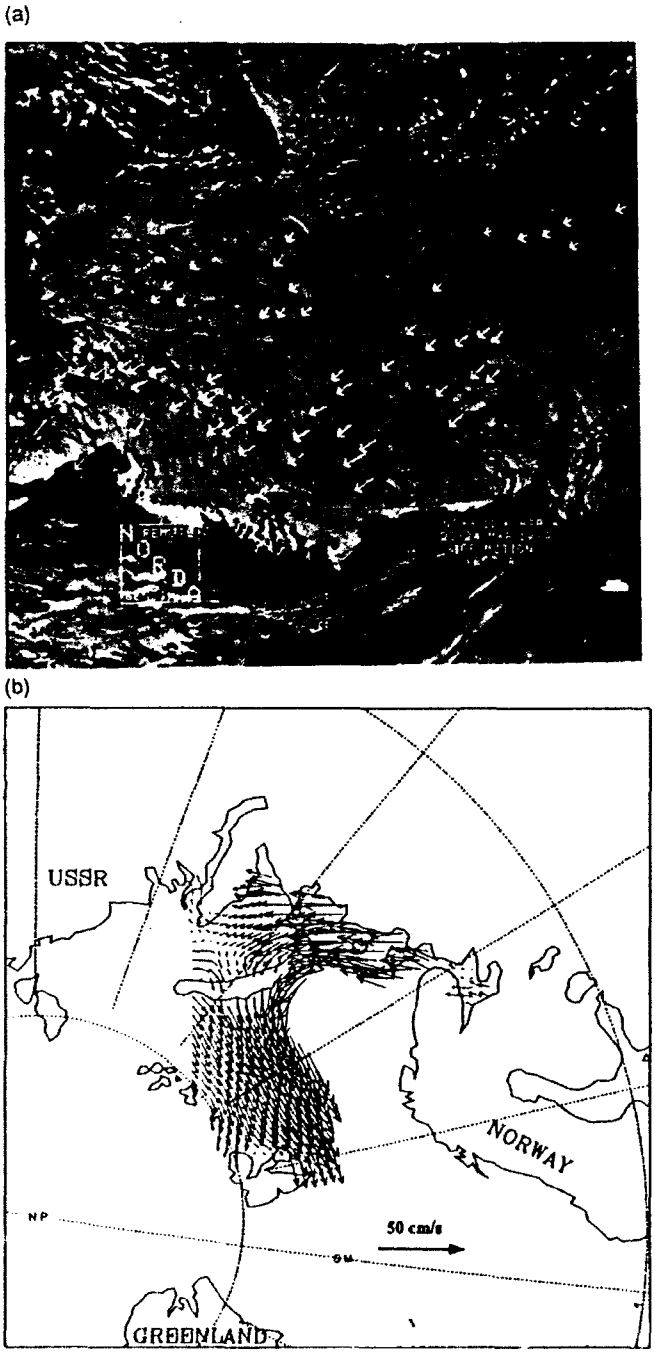

Fig. 22-8. Ice drift derived from (a) successive AVHRR images from March 23 and 24, 1989, and (b) the 24-hour forecast of RPIPS-B for the same time period.

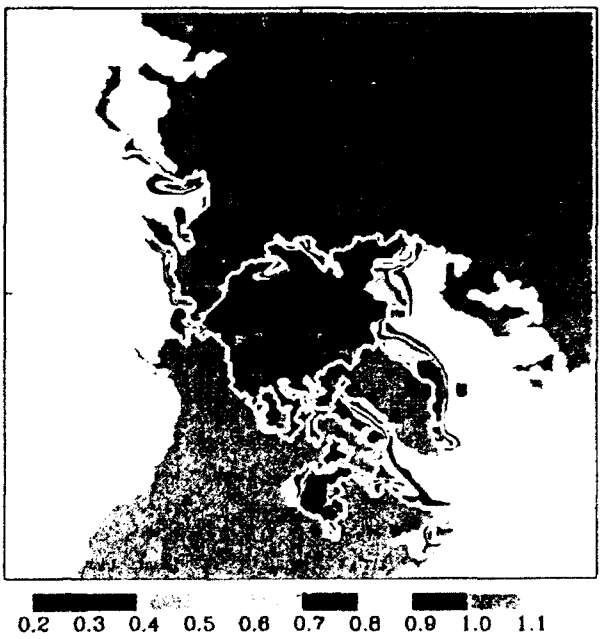

Fig. 22-9. PIPS 2.0 monthly mean ice concentration for March 1986.

tion coverage of sea ice conditions via the Synthetic Aperture Radar. Considerable potential exists for the use of SAR data in model studies of the parameterization of thin ice and open water regions. In addition, SAR may help provide more realistic parameterizations of the surface–atmosphere heat exchange, thereby serving as a stimulus to the coupling of ice and atmosphere models, as well as atmosphere–ice–ocean models.

Although large quantities of remotely sensed data already exist, there is great expectation for what will be available in the future. It is anticipated that remotely sensed data will provide additional important information to models on such variables as albedo, ice surface temperature, snow cover, ocean surface temperature, and atmospheric properties such as cloud cover, wind speed, and radiation budgets.

Although the interaction between data and models has been ongoing for many years, the future would suggest an even greater opportunity for interplay between the two. The combination of new sources of remotely sensed data and new products derived from these data should assist in the evolution of improved formulations for dynamic and thermodynamic processes affecting sea ice. These new formulations will be used to create more sophisticated models of the interaction between atmosphere, ice, and ocean. In addition, recent work by Thomas and Rothrock [1989], in Chapter 23, and the work presently being done by the U.S. Navy, suggests that the assimilation of data into models can provide both improved models as well as improved forecasts of sea ice conditions.

Acknowledgments.

John Walsh was supported by NASA's Interdisciplinary Research Program through grant IDP-88-009. James Maslanik was supported by NOAA's Climate and Global Change Program through grant NA85RAH05066. Ruth Preller was funded through the Navy Ocean Modeling and Prediction program by the Office of Naval Technology (program element 62435N) and by the U.S. Space and Naval Warfare Systems Command (program element 63207N). This book chapter, NRL contribution BC 001-92-322, is approved for public release; distribution unlimited.

REFERENCES

Aagaard, K. and E. C. Carmack, The role of sea ice and other fresh water in the Arctic circulation, *Journal of Geophysical Research, 94,* pp. 14,485–14,498, 1989.

Aagaard, K., J. H. Swift, and E. C. Carmack, Thermohaline circulation in the Arctic Mediterranean seas, *Journal of Geophysical Research, 90,* pp. 4833–4846, 1985.

Andreas, E. L., Comment on "Atmospheric boundary layer modification in the marginal ice zone" by T. J. Bennett, Jr., and K. Hunkins, *Journal of Geophysical Research, 92(C4),* pp. 3965–3968, 1987.

Andreas, E. L. and B. Murphy, Bulk transfer coefficients for heat and momentum over leads and polynyas, *Journal of Physical Oceanography, 16(11),* pp. 1875–1883, 1986.

Barkstrom, B. R. and G. L. Smith, The Earth Radiation Budget Experiment (ERBE): Science and implementation, *Review of Geophysics, 24,* pp. 379–390, 1986.

Barry, R. G., R. G. Crane, A. Schweiger, and J. Newell, Arctic cloudiness in spring from satellite imagery, *Journal of Climatology, 7,* pp. 423–451, 1987.

Barton, I. J., Transmission model and ground-truth investigation of satellite-derived sea surface temperatures, *Journal of Climate and Applied Meteorology, 24,* pp. 508–516, 1985.

Bauer, J. and S. Martin, A model of grease ice growth in small leads, *Journal of Geophysical Research, 88(C5),* pp. 2917–2925, 1983.

Bennett, T. J., Jr., and K. Hunkins, Atmospheric boundary layer modification in the marginal ice zone, *Journal of Geophysical Research, 91,* pp. 13,033–13,044, 1986.

Bjork, G., A one-dimensional time-dependent model for the vertical stratification of the upper Arctic Ocean, *Journal of Physical Oceanography, 19,* pp. 52–67, 1989.

Bourke, R. H. and A. S. McLaren, Contour mapping of Arctic Basin ice draft and roughness parameters, *Journal of Geophysical Research,* in press, 1992.

Bryan, K., Climate and the ocean circulation: III. The ocean model, *Monthly Weather Review, 97,* pp. 806–827, 1969.

Bryan, K., S. Manabe, and R. L. Pacanowski, A global ocean–atmosphere climate model. Part II. The ocean circulation, *Journal of Physical Oceanography, 5,* pp. 30–46, 1975.

Burns, B. A., D. J. Cavalieri, M. R. Keller, W. J. Campbell, T. C. Grenfell, G. A. Maykut, and P. Gloersen, Multisensor comparison of ice concentration estimates in the marginal ice zone, *Journal of Geophysical Research, 92,* pp. 6843–6856, 1987.

Cavalieri, D. J., P. Gloersen, and W. J. Campbell, Determination of sea ice parameters with the Nimbus 7 SMMR, *Journal of Geophysical Research, 89,* pp. 5355–5369, 1984.

Chang, A. T. C., J. L. Foster, and D. K. Hall, Nimbus-7 SMMR derived global snow cover parameters, *Annals of Glaciology, 9,* pp. 39–45, 1987.

Chu, P. C., An ice breeze mechanism for an ice divergence–convergence criterion in the marginal ice zone, *Journal of Physical Oceanography, 17(10),* pp. 1627–1632, 1987.

Colbeck, S. C., The layered character of snow covers, *Reviews of Geophysics, 29(1),* pp. 81–96, 1991.

Comiso, J. C., Sea ice effective microwave emissivities from satellite passive microwave and infrared observations, *Journal of Geophysical Research, 88,* pp. 7686–7704, 1983.

Comiso, J. C., Characteristics of Arctic winter sea ice from satellite multispectral microwave observations, *Journal of Geophysical Research, 91(C1),* pp. 975–994, 1986.

Comiso, J. C., Arctic multiyear ice classification and summer ice cover using passive microwave satellite data, *Journal of Geophysical Research, 95,* pp. 13,411–13,422, 1990.

Condal, A. R. and H. V. Le, Automated computer monitoring sea-ice temperature by use of NOAA satellite data, *Proceedings of the Eighth Canadian Symposium on Remote Sensing,* pp. 145–150, Montreal, Quebec, 1984.

Curlander, J. C., B. Holt, and K. J. Hussey, Determination of sea ice motion using digital SAR imagery, *IEEE Journal of Oceanic Engineering, OE-10(4),* pp. 358–367, 1985.

Ebert, E., Analysis of polar clouds from satellite imagery using pattern recognition and a statistical cloud analysis scheme, *Journal of Applied Meteorology, 28,* pp. 382–399, 1989.

Ebert, E. E. and J. A. Curry, Annual cycle of cloud radiative forcing over the Arctic Ocean, *Proceedings of the Seventh Conference on Atmospheric Radiation,* pp. 395–400, American Meteorological Society, Boston, Massachusetts, 1990.

Ellingson, R. G., D. J. Yanuk, H.-T. Lee, and A. Gruber, A technique for estimating outgoing long-wave radiation from HIRS radiance observations, *Journal of Atmospheric and Oceanic Technology, 6,* pp. 706–711, 1989.

Emery, W. J., C. W. Fowler, J. Hawkins, and R. H. Preller, Fram Strait satellite image-derived ice motions, *Journal of Geophysical Research, 96,* pp. 4751–4768, 1991.

Fichefet, T. and P. Gaspar, A model of upper ocean–sea ice interaction, *Journal of Physical Oceanography, 18(2),* pp. 181–195, 1988.

Flato, G. M. and W. D. Hibler, III, The effect of ice pressure on marginal ice zone dynamics, *IEEE Transactions on Geoscience and Remote Sensing, 27(5),*, pp. 514–521, 1989.

Fleming, G. H. and A. J. Semtner, Jr., A numerical study of interannual ocean forcing on Arctic sea ice, *Journal of Geophysical Research, 96,* pp. 4589–4604, 1991.

Fye, F. K., *The AFGWC automated cloud analysis model,* 97 pp., Technical Memorandum 78-002, United States Air Force, Offut Air Force Base, Nebraska, 1978.

Gabison, R., A thermodynamic model of the formation, growth, and decay of first-year sea ice, *Journal of Glaciology, 33(113),* pp. 105–119, 1987.

Gloersen, P. and W. J. Campbell, Variations in the Arctic, Antarctic, and global sea ice cover during 1978–1987 as observed with the Nimbus 7 Scanning Multichannel Microwave Radiometer, *Journal of Geophysical Research, 93,* pp. 10,666–10,674, 1988.

Gruber, A. and H. Jacobowitz, The long-wave radiation estimated from NOAA polar orbiting satellites: An update and comparison with Nimbus 7 ERB results, *Advanced in Space Research, 5(6),* pp. 111–120, 1985.

Hakkinen, S., Coupled ice–ocean dynamics in the marginal ice zones: Up/downwelling and eddy generation, *Journal of Geophysical Research, 91,* pp. 819–832, 1986.

Harvey, L. D. D., A semi-analytic energy balance climate model with explicit sea ice and snow physics, *Journal of Climatology, 1,* pp. 1065–1085, 1988.

Henderson–Sellers, A., *Satellite Sensing of a Cloudy Atmosphere: Observing the Third Planet,* 340 pp., Taylor & Francis Inc., Philadelphia, 1984.

Henderson–Sellers, A. and K. McGuffie, Are cloud amounts estimated from satellite sensor and conventional surface-based observations related?, *International Journal of Remote Sensing, 11(3),* pp. 543–550, 1990.

Henderson–Sellers, A. and M. F. Wilson, Surface albedo data for climate modeling, *Reviews of Geophysics and Space Physics, 21,* pp. 1743–1778, 1983.

Hibler, W. D., III, A dynamic-thermodynamic sea ice model, *Journal of Physical Oceanography, 9,* pp. 815–846, 1979.

Hibler, W. D., III, Modeling a variable thickness sea ice cover, *Monthly Weather Review, 108,* pp. 1943–1973, 1980a.

Hibler, W. D., III, Sea ice growth, drift and decay, in *Dynamics of Snow and Ice Masses,* edited by S. C. Colbeck, 468 pp., Academic Press, New York, 1980b.

Hibler, W. D., III, Ice dynamics, in *The Geophysics of Sea Ice,* edited by N. Untersteiner, pp. 577–640, NATO ASI Series B: Physics vol. 146, Plenum Press, New York, 1986.

Hibler, W. D., III and S. F. Ackley, Numerical simulation of the Weddell Sea pack ice, *Journal of Geophysical Research, 88,* pp. 2873–2887, 1983.

Hibler, W. D., III and K. Bryan, Ocean circulation: Its effects on seasonal sea-ice simulations, *Science, 224,* pp. 489–491, 1984.

Hibler, W. D., III and K. Bryan, A diagnostic ice–ocean model, *Journal of Physical Oceanography, 17,* pp. 987–1015, 1987.

Hibler, W. D., III and J. E. Walsh, On modeling seasonal and interannual fluctuations of Arctic sea ice, *Journal of Physical Oceanography, 12,* pp. 1514–1523, 1982.

Ikeda, M., A coupled ice–ocean model of a wind driven coastal flow, *Journal of Geophysical Research, 90,* pp. 9119–9128, 1985.

Ikeda, M., A three-dimensional coupled ice–ocean model of coastal circulation, *Journal of Geophysical Research, 93,* pp. 10,731–10,748, 1988.

Jacobowitz, H., H. V. Soule, H. L. Kyle, F. House, and the Nimbus-7 ERB Experiment Team, The Earth Radiation Budget (ERB) Experiment—An Overview, *Journal of Geophysical Research, 89(D4),* pp. 5021–5038, 1984.

Kantha, L. H. and G. L. Mellor, Application of a two-dimensional coupled ocean–ice model to the Bering Sea marginal ice zone, *Journal of Geophysical Research, 94,* pp. 10,921–10,935, 1989.

Key, J. and R. G. Barry, Cloud cover analysis with Arctic AVHRR data, 1. Cloud detection, *Journal of Geophysical Research, 94(D15),* pp. 18,521–18,535, 1989.

Kneizys, F. X., E. P. Shettle, L. W. Abreu, J. H. Chetwynd, G. P. Anderson, W. O. Gallery, J. E. A. Selby, and S. A. Clough, *Users Guide to LOWTRAN-7,* document AFGL-TR-88-00177, 138 pp., Air Force Geophysics Laboratory, Hanscom Air Force Base, Massachusetts, 1988.

Koch, C., A coupled sea ice atmospheric boundary layer model. Part 1: Description of the model and 1979 standard run, *Beitraege zur Physik der Atmosphaere, 61(4),* pp. 344–354, 1988.

Kopia, L. P., Earth Radiation Budget Experiment scanner instrument, *Review of Geophysics, 24,* pp. 400–406, 1986.

Kozo, T. L., Initial model results for Arctic mixed layer circulation under a refreezing lead, *Journal of Geophysical Research, 88(C5),* pp. 2926–2934, 1983.

Ledley, T. S., A coupled energy balance climate–sea ice model: Impact of sea ice and leads on climate, *Journal of Geophysical Research, 93,* pp. 15,915–15,932, 1988.

Ledley, T. S., The climatic response to meridional sea-ice transport, *Journal of Climate, 4,* pp. 147–163, 1991.

Lemke, P., A coupled one-dimensional sea ice–ocean model, *Journal of Geophysical Research, 92,* pp. 13,164–13,172, 1987.

Lemke, P. and T. O. Manley, The seasonal variation of the mixed layer and the pycnocline under polar sea ice, *Journal of Geophysical Research, 89(C4),* pp. 6494–6504, 1984.

Lemke, P., E. W. Trinkl, and K. Hasselmann, Stochastic dynamic analysis of polar sea ice variability, *Journal of Physical Oceanography, 10,* pp. 2100–2120, 1980.

Manabe, S. and R. J. Stouffer, Two stable equilibria of a coupled ocean–atmosphere model, *Journal of Climate, 1,* pp. 841–866, 1988.

Manabe, S., K. Bryan, and M. J. Spelman, A global ocean–atmosphere climate model with seasonal variation for future studies for climate sensitivity, *Dynamics of Atmospheres and Oceans, 3,* pp. 393–426, 1979.

Martinson, D. G., P. D. Killworth, and A. L. Gordon, A convective model for the Weddell polynya, *Journal of Physical Oceanography, 11,* pp. 466–488, 1981.

Maykut, G. A., Energy exchange over young sea ice in the Central Arctic, *Journal of Geophysical Research, 83,* pp. 3646–3658, 1978.

Maykut, G. A., Large-scale heat exchange and ice production in the Central Arctic, *Journal of Geophysical Research, 87,* pp. 7971–7984, 1982.

Maykut, G. A. and N. Untersteiner, Some results from a time-dependent thermodynamic model of sea ice, *Journal of Geophysical Research, 76,* pp. 1550–1575, 1971.

McClain, E. P., W. G. Pichel, and C. C. Walton, Comparative performance of AVHRR-based multichannel sea surface temperatures, *Journal of Geophysical Research, 90(C6),* pp. 11,587–11,601, 1985.

McGuffie, K., R. G. Barry, J. Newell, A. Schweiger, and D. A. Robinson, Intercomparison of satellite-derived cloud analyses for the Arctic Ocean in spring and summer, *International Journal of Remote Sensing, 9,* pp. 447–467, 1988.

Mellor, G. L. and L. Kantha, An ice–ocean coupled model, *Journal of Geophysical Research, 94,* pp. 10,937–10,954, 1989.

Minnett, P. J., The regional optimization of infrared measurements of sea surface temperature from space, *Journal of Geophysical Research, 95(C8),* pp. 13,497–13,510, 1990.

Morris, E. M., Turbulent transfer over snow and ice, *Journal of Hydrology, 105(314),* pp. 205–223, 1989.

Motoi, T., N. Ono, and M. Wakatsuchi, A mechanism for the formation of the Weddell polynya in 1974, *Journal of Physical Oceanography, 17,* pp. 2241–2247, 1987.

Overland, J. E., Atmospheric boundary layer structure and drag coefficients over sea ice, *Journal of Geophysical Research, 90,* pp. 9029–9049, 1985.

Overland, J. E., A model of the atmospheric boundary layer over sea ice during winter, *Second Conference on Polar Meteorology and Oceanography,* pp. 69–72, American Meteorological Society, Madison, Wisconsin, 1988.

Overland, J. E., R. M. Reynolds, and C. H. Pease, A model of the atmospheric boundary layer over the marginal ice zone, *Journal of Geophysical Research, 88(C5),* pp. 2836–2840, 1983.

Parkinson, C. L., On the development and cause of the Weddell polynya in a sea ice simulation, *Journal of Physical Oceanography, 13,* pp. 501–511, 1983.

Parkinson, C. L. and R. A. Bindschadler, Response of Antarctic sea ice to atmospheric temperature increases, in *Climate Processes and Climate Sensitivity, vol. 5,* edited by J. E. Hanson and T. Takahashi, pp. 254–264, American Geophysical Union, Washington, DC, 1984.

Parkinson, C. L. and G. F. Herman, Sea ice simulations based on fields generated by the GLAS GCM, *Monthly Weather Review, 108,* pp. 2080–2091, 1980.

Parkinson, C. L. and W. M. Washington, A large-scale numerical model of sea ice, *Journal of Geophysical Research, 84(C1),* pp. 311–337, 1979.

Parkinson, C. L., J. C. Comiso, H. J. Zwally, D. J. Cavalieri, P. Gloersen, and W. J. Campbell, *Arctic Sea Ice, 1973–1976: Satellite-Passive Microwave Observations,* NASA SP-489, 296 pp., National Aeronautics and Space Administration, Washington, DC, 1987.

Pease, C. H. and J. E. Overland, An atmospherically driven sea-ice drift model for the Bering Sea, *Annals of Glaciology, 5,* pp. 111–114, 1984.

Piacsek, S., R. Allard, and A. Warn–Varnas, Studies of the Arctic ice cover and upper ocean with a coupled ice–ocean model, *Journal of Geophysical Research, C3,* pp. 4631–4650, 1991.

Pollard, D., M. L. Batteen, and Y. Han, Development of a simple upper-ocean sea-ice model, *Journal of Physical Oceanography, 13,* pp. 754–768, 1983.

Preller, R. H., *The NORDA / FNOC Polar Ice Prediction System (PIPS)—Arctic: A Technical Description,* 60 pp., NORDA Report 108, Naval Oceanographic and Atmospheric Research Laboratory, Stennis Space Center, Mississippi, 1985.

Preller, R. H. and P. G. Posey, *The Polar Ice Prediction System—A Sea Ice Forecasting System,* NORDA Report 212, 45 pp., Naval Oceanographic and Atmospheric Research Laboratory, Stennis Space Center, Mississippi, 1989.

Preller, R. H., S. Riedlinger, and P. G. Posey, *The Regional Polar Ice Prediction Systems Barents Sea (RPIPS-B): A Technical Description*, NORDA Report 182, 38 pp., Naval Oceanographic and Atmospheric Research Laboratory, Stennis Space Center, Mississippi, 1989.

Preller, R. H., A. Cheng, and P. G. Posey, Preliminary testing of a sea ice model of the Greenland Sea, in *Proceedings of the W. F. Weeks Sea Ice Symposium*, CRREL Monograph 90-1, 19 pp., USA Cold Regions Research and Engineering Laboratory, Hanover, New Hampshire, 1990.

Pritchard, R. S., editor, *Sea Ice Processes and Models*, 474 pp., University of Washington Press, Seattle, Washington, 1980.

Ramanathan, V., R. D. Cess, E. F. Harrison, P. Minnis, B. R. Barkstrom, E. Ahmad, and D. Hartmann, Cloud-radiative forcing and climate: Results from the Earth Radiation Budget Experiment, *Science, 243*, pp. 57–63, January 6, 1989.

Raymo, R. E., D. Rind, and W. F. Ruddiman, Climatic effects of reduced Arctic sea ice limits in the GISS II general circulation model, *Paleoceanography, 5*, pp. 367–382, 1990.

Riedlinger, S. H. and R. H. Preller, The development of a coupled ice–ocean model for forecasting ice conditions in the Arctic, *Journal of Geophysical Research, 96*, pp. 16,955–16,978, 1991.

Riedlinger, S. H. and A. Warn–Varnas, Predictions and studies with a one-dimensional ice–ocean model, *Journal of Physical Oceanography, 20*, pp. 1545–1562, 1990.

Robinson, D. A., G. Scharfen, M. C. Serreze, G. Kukla, and R. G. Barry, Snow melt and surface albedo in the Arctic Basin, *Geophysical Research Letters, 13(9)*, pp. 945–948, 1986.

Roed, L. P. and J. J. O'Brien, A coupled ice–ocean model of upwelling in the marginal ice zone, *Journal of Geophysical Research, 88*, pp. 2863–2872, 1983.

Ross, B. and J. E. Walsh, A comparison of simulated and observed fluctuations in Arctic surface albedo, *Journal of Geophysical Research, 92*, pp. 13,115–13,126, 1987.

Rossow, W. B. and R. A. Schiffer, ISCCP cloud data products, *Bulletin American Meteorological Society*, in press, 1991.

Rossow, W. B., F. Mosher, E. Kinsella, A. Arking, M. Desbois, E. Harrison, P. Minnis, E. Ruprecht, G. Seze, C. Simmer, and E. Smith, ISCCP cloud algorithm comparison, *Journal of Climate and Applied Meteorology, 24*, pp. 877–903, 1985.

Rossow, W. B., C. L. Brest, and L. C. Gardner, Global, seasonal and surface variations from satellite radiance measurements, *Journal of Climate, 2*, pp. 214–247, 1989.

Rothrock, D. A. and D. R. Thomas, The Arctic Ocean multiyear ice balance, 1979–1982, *Annals of Glaciology, 14*, pp. 252–255, 1990.

Scharfen, G., R. G. Barry, D. A. Robinson, G. Kukla, and M. C. Serreze, Large-scale patterns of snow melt on Arctic sea ice mapped from meteorological satellite imagery, *Annals of Glaciology, 9*, pp. 1–6, 1987.

Schluessel, P. and H. Grassl, SST in polynyas: A case study, *International Journal of Remote Sensing, 11(6)*, pp. 933–945, 1990.

Schluessel, P., H.-Y. Shin, W. J. Emery, and H. Grassl, Comparison of satellite-derived sea surface temperatures with in situ skin temperatures, *Journal of Geophysical Research, 92(C3)*, pp. 2859–2874, 1987.

Schwerdtfeger, P. and G. E. Weller, Radiative heat transfer processes in snow and ice, in *Meteorological Studies at Plateau Station, Antarctica*, edited by J. A. Businger, pp. 27–34, Antarctic Research Series 25, American Geophysical Union, Washington, DC, 1977.

Semtner, A. J., Jr., A model for the thermodynamic growth of sea ice in numerical investigations of climate, *Journal of Physical Oceanography, 6(3)*, pp. 379–389, 1976.

Semtner, A. J., Jr., A numerical study of sea ice and ocean circulation in the Arctic, *Journal of Physical Oceanography, 17*, pp. 1077–1099, 1987.

Serreze, M. C. and M. C. Rehder, June cloud cover over the Arctic Ocean, *Geophysical Research Letters, 17(12)*, pp. 2397–2400, 1990.

Serreze, M. C., R. G. Barry, and A. S. McLaren, Seasonal variations in the sea ice motion and effects on sea ice concentration in the Canada Basin, *Journal of Geophysical Research, 94*, pp. 10,955–10,970, 1989.

Serreze, M. C., J. A. Maslanik, R. H. Preller, and R. G. Barry, Sea ice concentrations in the Canada Basin during 1988: Comparisons with other years and evidence of multiple forcing mechanisms, *Journal of Geophysical Research, 95(C12)*, pp. 22,253–22,268, 1990.

Shine, K. P. and A. Henderson–Sellers, The sensitivity of a thermodynamic sea ice model to changes in surface albedo parameterization, *Journal of Geophysical Research, 90(D1)*, pp. 2243–2250, 1985.

Simmonds, I. and W. F. Budd, A simple parameterization of ice leads in a general circulation model and the sensitivity of climate to change in Antarctic ice concentration, *Annals of Glaciology, 14*, pp. 266–269, 1990.

Smith, D. C. and A. Bird, The interaction of an ocean eddy with an ice edge ocean jet in a marginal ice zone, *Journal of Geophysical Research, C3*, pp. 4675–4689, 1991.

Smith, D. C., A. Bird, and P. Budgell, A numerical study of mesoscale ocean eddy interaction with marginal ice zone, *Journal of Geophysical Research, 93*, pp. 12,461–12,473, 1988.

Smith, S. D., R. D. Muench, and C. H. Pease, Polynyas and leads: An overview of physical processes and environment, *Journal of Geophysical Research, 95(C6)*, pp. 9461–9479, 1990.

Steffen, K. and J. A. Maslanik, Comparison of Nimbus 7 Scanning Multichannel Microwave Radiometer radiance and derived sea ice concentrations with Landsat imagery for the North Water area of Baffin Bay, *Journal of Geophysical Research, 93(C9),* pp. 10,769–10,781, 1988.

Steffen, K. and A. J. Schweiger, A multisensor approach to sea ice classification for the validation of DMSP-SSM/I passive microwave derived sea ice products, *Photogrammetric Engineering and Remote Sensing, 56(1),* pp. 75–82, 1990.

Stossel, A., P. Lemke, and B. Owens, *Coupled Sea Ice Mixed Layer Simulations for the Southern Ocean,* 29 pp., Report Number 30, Max-Planck-Institut fuer Meteorologie, Hamburg, Germany, 1989.

Stowe, L. L., C. G. Wellemeyer, T. F. Eck, H. Y. M. Yeh, and Nimbus-7 Cloud Data Processing Team, Nimbus-7 global cloud climatology. Part I: Algorithms and validations, *Journal of Climate, 1,* pp. 445–470, 1988.

Susskind, J. and D. Reuter, Retrieval of sea surface temperatures from HIRS2/MSU, *Journal of Geophysical Research, 90(C6),* pp. 11,602–11,608, 1985.

Swift, C. T. and D. J. Cavalieri, Passive microwave remote sensing for sea ice research, *Eos, 66(49),* pp. 1210–1212, 1985.

Tang, C. L., A two-dimensional thermodynamic model for sea ice advance and retreat in the Newfoundland marginal ice zone, *Journal of Geophysical Research, C3,* pp. 4723–4737, 1991.

Thomas, D. R. and D. A. Rothrock, Blending sequential scanning multichannel microwave radiometer and buoy data into a sea ice model, *Journal of Geophysical Research, 94,* pp. 10,907–10,920, 1989.

Thorndike, D. S., A naive zero-dimensional sea ice model, *Journal of Geophysical Research, 93,* pp. 5095–5099, 1988.

Tian, L. and J. A. Curry, Cloud overlap statistics, *Journal of Geophysical Research, 94(D7),* pp. 9925–9935, 1989.

Tucker, W. B., *Application of a Numerical Sea Ice Model to the East Greenland Area,* CRREL Report 82-16, 40 pp., USA Cold Regions Research and Engineering Laboratory, Hanover, New Hampshire, 1982.

Turner, J. and D. E. Warren, Cloud track winds in the polar regions from sequences of AVHRR images, *International Journal of Remote Sensing, 10(4 and 5),* pp. 695–703, 1989.

Untersteiner, N., On the mass and heat budget of the Arctic sea ice, *Archiv fuer Meteorologie, Geophysik, und Bioklimatologie, A(12),* pp. 151–182, 1961.

Walsh, J. E. and W. L. Chapman, Short term climate variability of the Arctic, *Journal of Climate, 3,* pp. 237–250, 1991.

Walsh, J. E., W. D. Hibler, III, and B. Ross, Numerical simulation of northern hemisphere sea ice variability: 1951–1980, *Journal of Geophysical Research, 90,* pp. 4847–4865, 1985.

Walsh, J. E. and H. J. Zwally, Multiyear sea ice in the Arctic: Model- and satellite-derived, *Journal of Geophysical Research, 95,* pp. 11,613–11,628, 1990.

Weller, G. and P. Schwerdtfeger, Thermal properties and heat transfer processes of low-temperature snow, in *Meteorological Studies at Plateau Station, Antarctica,* edited by J. A. Businger, pp. 27–34, Antarctic Research Series 25, American Geophysical Union, Washington, DC, 1977.

Wohl, G., Sea ice edge forecast verification program for the Bering Sea, *National Weather Digest, 16(4),* pp. 6–12, 1991.

Wood, R. G. and L. A. Mysak, A simple ice–ocean model for the Greenland Sea, *Journal of Physical Oceanography, 19(12),* pp. 1865–1880, 1989.

Zwally, H. J. and J. E. Walsh, Comparison of observed and modeled ice motion in the Arctic Ocean, *Annals of Glaciology, 9,* pp. 136–144, 1987.

Zwally, H. J., J. C. Comiso, C. L. Parkinson, W. J. Campbell, F. D. Carsey, and P. Gloersen, *Antarctic Sea Ice, 1973–1976: Satellite Passive-Microwave Observations,* NASA SP-459, 206 pp., National Aeronautics and Space Administration, Washington, DC, 1983.